https://doi.org/10.59761/RCR5204

Modification of black phosphorus with metal substrates: towards single-atom catalysts

Aidar M. Kuchkaev,[a]* Vladislav S. Kashansky,[a,b] Airat M. Kuchkaev,[a] Aleksandr V. Sukhov,[a,b] Xiongwu Kang,[c] Oleg G. Sinyashin,[a] Dmitry G. Yakhvarov[a,b]*

[a] *Arbuzov Institute of Organic and Physical Chemistry, FRC Kazan Scientific Center of RAS, 420088 Kazan, Russia*
[b] *Alexander Butlerov Institute of Chemistry, Kazan Federal University, 420008 Kazan, Russia*
[c] *New Energy Research Institute, School of Environment and Energy, South China University of Technology, Higher Education Mega Center, 510006 Guangzhou, China*

Owing to its unique anisotropic structure, high charge carrier mobility, and tunable bandgap, few-layer black phosphorus (FLBP) emerges as a highly promising material for applications in micro- and optoelectronics, energy conversion, and catalysis. Chemical functionalization and structural modification of FLBP not only enhance its ambient stability but also enable precise tailoring of its electronic and catalytic properties. This review systematizes state-of-the-art methods for the synthesis of FLBP and its surface modification using metal substrates. Special emphasis is placed on the fabrication strategies of 0D/2D FLBP-based nanocomposites decorated with transition metal nanoparticles, the modification of FLBP with single metal atoms, and the application of these materials in electrocatalytic and photocatalytic processes, including the hydrogen evolution, CO_2 reduction and nitrogen fixation. In conclusion, the key challenges and future research directions in the development of novel FLBP-based catalytic systems for practical energy and environmental catalysis applications are outlined.
The bibliography includes 214 references.
Keywords: black phosphorus, phosphorene, nanomaterials, transition metal nanoparticles, single-atom catalysts, electrocatalysis, photocatalysis, hydrogen evolution reaction, CO_2 reduction, nitrogen fixation.

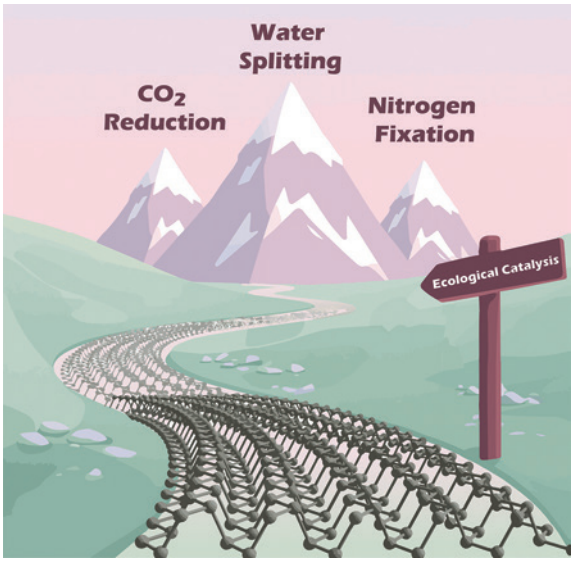

Contents

1. Introduction

In recent decades, two-dimensional (2D) materials have attracted increasing attention due to their unique physical and chemical properties and broad application potential.[1,2] The discovery of graphene in 2004,[3] a key milestone in modern materials science, provided the impetus for a thorough study of these materials. This achievement not only demonstrated the fundamental possibility of the existence of stable single-atom layers but also stimulated the search for other two-dimensional structures with unique properties.[4] Among the most promising materials in this class, black phosphorus (BP), an allotropic modification of phosphorus with a layered graphite-like structure,[5,6] occupies a special place. Individual layers of black phosphorus are held together by weak van der Waals forces, allowing for the production of 2D materials based thereon. The ideal 2D modification, phosphorene, is a monoatomic layer of black phosphorus with a characteristic puckered structure. In practice, few-layer black phosphorus (FLBP) is more commonly used. It consists of several (usually 2 to 30) weakly bonded layers of BP,

Received 25 September 2025

retaining the key properties of a monolayer while being more readily available.[7,8]

The experimental production of phosphorene and FLBP in 2014 boosted the development of this scientific field.[9–12] The increased interest of researchers was driven by the unique characteristics of these materials such as pronounced structural anisotropy, tunable semiconducting properties, high charge carrier mobility and high biocompatibility. Owing to these properties, FLBP-based 2D materials have found application in a variety of devices, from electro- and photocatalysts, lithium- and sodium-ion batteries to field-effect transistors, laser devices, solar cells and biomedical materials.[5,7,13–15]

However, the widespread adoption of FLBP is hampered by its high sensitivity to oxygen and atmospheric moisture, leading to rapid oxidation of the material under ambient conditions.[8,16–21] The primary solution to the problem of FLBP stability is chemical modification of its surface.[22–24] Importantly, such approaches not only increase the material's oxidation resistance but also allow for targeted modification of its functional properties. Of particular interest are hybrid systems based on FLBP and nanoparticles, as well as transition metal-containing atomic and molecular moieties demonstrating a synergistic effect due to the combination of the advantages of the two-dimensional FLBP structure and the catalytic properties of metal components.

This review summarizes current strategies for FLBP modification with metal-containing substrates and their applications in photocatalytic and electrocatalytic processes. Unlike existing publications,[24–27] this paper focuses on an in-depth examination of recent advances and an assessment of the potential of using FLBP as a unique platform for creating single-atom catalysts. The performance of the resulting hybrid materials is demonstrated in key processes of sustainable energy and eco-catalysis, such as hydrogen and oxygen evolution reactions, carbon dioxide reduction and nitrogen fixation. The correlations between the structural features of modified materials and their functional properties were analyzed in detail, which forms the basis for the targeted design of efficient catalysts based on FLBP.

2. Structure and properties of black phosphorus

Black phosphorus is a layered graphite-like material in which individual layers are held together by weak van der Waals interactions with a characteristic interlayer distance of 5.3 Å (Fig. 1). Unlike graphene with a flat hexagonal lattice and sp^2-hybridized carbon atoms, black phosphorus consists of sp^3-hybridized phosphorus atoms, which imparts an unusual folded structure to the material.[10,28,29] This structure leads to the formation of two different structural directions in the $x–y$ plane: the 'armchair' and 'zigzag', and determines unique in-plane anisotropy of the electronic, optical and mechanical properties. For example, the thermal conductivity along the zigzag direction (110 W m^{-1} K^{-1} at 300 K) is three times higher than that along the armchair direction (36 W m^{-1} K^{-1}),[15] while the mobility of charge carriers, on the contrary, is maximum along the armchair axis.[12,30] Differences in electrical conductivity also affect the optical properties of the material: in the infrared range (2–5 μm), the absorption of light polarized along the armchair direction is approximately 1.5 times stronger than that for the zigzag one.[30,31] The different orientations of phosphorus–phosphorus covalent bonds in the crystal lattice give rise to pronounced anisotropy of mechanical properties: Young's modulus in the zigzag direction (106.4 GPa) is several times higher than that along the armchair direction (41.3 GPa), which is due to the more efficient distribution of strains during the BP

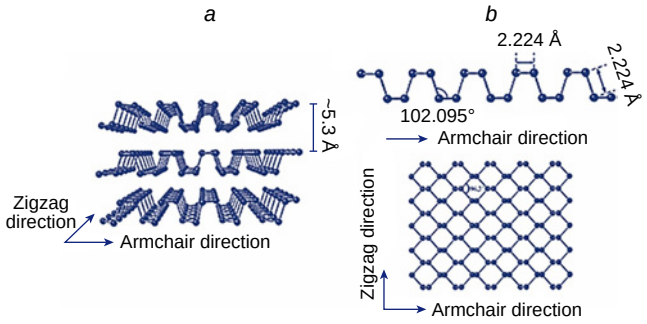

Figure 1. Black phosphorus (*a*) and phosphorene (*b*) crystal structure.[29] Published under a CC-BY-NC-ND license from Elsevier.

Aidar M.Kuchkaev. PhD in Chemistry, Junior Researcher at the Arbuzov Institute of Organic and Physical Chemistry, FRC Kazan Scientific Center of RAS. E-mail: kuchkaev95@mail.ru
Current research interests: black phosphorus, phosphorene, nanomaterials, electrocatalysis, photocatalysis.
V.S.Kashansky. PhD Student at the Arbuzov Institute of Organic and Physical Chemistry, FRC Kazan Scientific Center of RAS; Engineer at the Alexander Butlerov Institute of Chemistry, Kazan Federal University. E-mail: vladkashansky@gmail.com
Current research interests: black phosphorus, phosphorene, nanomaterials.
Airat M.Kuchkaev. PhD in Chemistry, Junior Researcher at the Arbuzov Institute of Organic and Physical Chemistry, FRC Kazan Scientific Center of RAS. E-mail: 95ka@bk.ru
Current research interests: elemental phosphorus, transition metal complexes, nanomaterials, catalysis.
A.V.Sukhov. PhD in Chemistry, Researcher at the Arbuzov Institute of Organic and Physical Chemistry, FRC Kazan Scientific Center of RAS and the Alexander Butlerov Institute of Chemistry, Kazan Federal University. E-mail: alex.suhoff@rambler.ru
Current research interests: black phosphorus, transition metal complexes, electrochemistry, electrocatalysis, homogeneous catalysis.
X.Kang. Doctor of Sciences in Chemistry, Professor at the New Energy Research Institute, School of Environment and Energy, South China University of Technology.
E-mail: esxkang@scut.edu.cn
Current research interests: electrocatalysts for hydrogen evolution and CO_2 reduction, nanomaterials, single-atom catalysts, black phosphorus.
O.G.Sinyashin. Academician of RAS, Doctor of Sciences in Chemistry, Scientific Director of the Arbuzov Institute of Organic and Physical Chemistry, FRC Kazan Scientific Center of RAS.
E-mail: oleg@iopc.ru
Current research interests: elemental phosphorus, organophosphorus compounds, catalysis, transition metal complexes, functional materials.
D.G.Yakhvarov. Corresponding Member of RAS, Doctor of Sciences in Chemistry, Chief Researcher at the Arbuzov Institute of Organic and Physical Chemistry, FRC Kazan Scientific Center of RAS and the Alexander Butlerov Institute of Chemistry, Kazan Federal University. E-mail: yakhvar@iopc.ru
Current research interests: elemental phosphorus, black phosphorus, transition metal complexes, electrochemistry, catalysis, nanomaterials.

Translation: N.M.Vinogradova.

deformation.[32,33] These unique properties open up wide possibilities for the application of BP in various devices. In electronics, the anisotropy of charge carrier mobility enables the creation of high-speed transistors with controlled current direction and reconfigurable circuits. The optical properties of the material make it promising for IR photodetectors and polarization sensors. Thermoelectric applications rely on the large difference in thermal conductivity in different directions, which can significantly improve energy conversion efficiency. Furthermore, mechanical anisotropy enables the development of specialized strain sensors and robust components for flexible electronics.[34]

In addition to anisotropy, BP is characterized by a strong dependence of the band gap on the number of layers. Its value varies from 0.3 eV for a bulk sample to 2.0 eV for a single layer, which allows for targeted tuning of the electronic and optical properties of BP-based materials.[6] High carrier mobility (up to ~ 1000 $cm^2\ V^{-1}\ s^{-1}$) coupled with a significant on/off current ratio (up to 10^5) makes this material particularly attractive for use in field-effect transistors and high-frequency electronics.[30] Furthermore, BP exhibits strong interaction with light over a wide spectral range, from visible to infrared radiation, opening up prospects for the creation of efficient photocatalysts, photodetectors, and next-generation optoelectronic devices.[30]

Despite the unique properties of phosphorene and FLBP, their use in micro- and optoelectronics is limited by their high sensitivity to atmospheric oxygen, which leads to oxidation of the material and deterioration of its physical properties. Lone electron pairs on the FLBP surface actively interact with oxygen, forming phosphorus oxides P_xO_y, which then react with water, converting to phosphoric acid.[16,18,21] As a result, the material quickly loses its crystallinity and electronic properties.

Favron *et al*.[21] showed that the oxidation of FLBP is promoted by light: excited electrons react with oxygen, forming reactive species, which in turn oxidize the phosphorus atoms of the material. The rate of this process depends linearly on the O_2 concentration and light intensity, and exponentially on the square of the band gap. This is because a broader band gap raises the energy of the conduction band minimum. The resulting higher-energy excited electrons possess greater reducing power, which significantly increases the probability of their interaction with oxygen, leading to an accelerated formation of reactive oxygen species.

Later, Wang and co-workers[17] proposed a three-step oxidation mechanism for FLBP. In the first step, oxygen reacts with light-excited electrons to generate the superoxide radical $O_2^{-\bullet}$. In the next step, $O_2^{-\bullet}$ dissociates on the FLBP surface and forms a P–O bond. In the third step, H_2O molecules bind to the P–O units and remove them from the surface.

It's important to note that the oxygen-induced degradation of FLBP is not always a negative factor. Moreover, the decomposition of FLBP to phosphoric acid and phosphate ions has given a powerful impetus to the development of a new approach to cancer therapy: bioactive phospho-therapy.[35,36] This method is based on the idea of delivering large quantities of biocompatible phosphate anions to cancer cells. Due to high levels of oxidative stress and accelerated energy metabolism, tumour cells rapidly cleave these compounds, providing an immediate and dramatic increase in intracellular phosphate concentrations. This unnatural spike violates the process of ATP hydrolysis and triggers apoptosis — the programmed death of cancer cells.[36] In addition to this effect, due to its ability to generate reactive oxygen species, strong absorption of light in the near-infrared range, and high biocompatibility, FLBP is considered to be a multifunctional and highly promising platform for photodynamic and photothermal therapy, as well as drug delivery, enabling a comprehensive impact on cancer cells.[37–40]

3. Preparation of crystalline black phosphorus

Crystalline phosphorus was first obtained by Bridgman[41] in 1914 by exposing white phosphorus to a pressure of ~ 1.2 GPa and a temperature of 200°C. However, due to the extremely drastic conditions of this method, a search subsequently began for alternative approaches that would allow for the production of BP under milder conditions. Thus, in 1943, Krebs *et al*.[42] developed a method according to which BP is formed by thermal treatment of white phosphorus at a temperature of 360–380°C and a pressure of 35–45 MPa in the presence of BP seed crystals and mercury metal, which acts as a catalyst. Furthermore, an approach was proposed for producing BP by crystallizing white phosphorus in molten bismuth. The crystals formed during this process were isolated by dissolving the bismuth matrix in nitric acid.[43] Despite high BP yields, this method has not found widespread application due to its high labor intensity, difficulty controlling crystallization conditions and problems associated with residual bismuth impurity content in the final product.

The most common laboratory method for synthesizing crystalline BP is the method developed by the Nilges research group.[44–48] The authors obtained BP *via* a gas-transport reaction using red phosphorus, an Au–Sn alloy, and SnI_4 as mineralizing agent.[44] For this purpose, the reagent mixture was sealed in a quartz ampoule and heated in a two-zone muffle furnace to 600–700°C, creating a small temperature gradient (Fig. 2). In this process, the BP is formed in the colder end of the ampoule by slowly cooling the reactants to 500°C. An improved method was subsequently developed in which only Sn and SnI_4 were used as mineralizing agents, which significantly reduced the cost of the synthesis procedure.[45] Further optimization of the process conditions made it possible to obtain BP crystals with a purity of up to 99.999%.[49]

Research is currently underway to develop industrially scalable approaches to the synthesis of BP. For example, Zhang *et al*.[50] reported an example of multi-gram synthesis of BP by reducing phosphorus pentachloride with aluminum metal at 300°C. This process produces BP flake-like nanostructures measuring 20–100 nm, forming aggregates approximately 2 μm in size.

4. Preparation of few-layer black phosphorus

There are two main approaches to producing FLBP, which differ in the use of different modifications of phosphorus: the 'top-down' method, *i.e*. formation as a result of exfoliation of BP, and the 'bottom-up' method based on the transformation of white or red phosphorus.

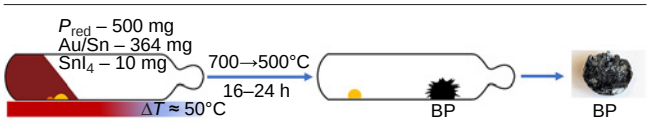

Figure 2. Scheme of the gas transport synthesis of black phosphorus.

4.1. 'Top-down' methods

4.1.1. Mechanical exfoliation

The Scotch tape method of mechanical exfoliation is widely used to produce various two-dimensional materials. This technology was first proposed for the isolation of graphene nanosheets,[3] and with the development of the field of science devoted to two-dimensional materials, it has begun to be successfully applied to other materials, including FLBP.[13,51–54] This method involves layer-by-layer exfoliation of BP using adhesive tape, followed by the transfer of the resulting layers onto a solid substrate (usually SiO_2/Si wafer). After the layers are transferred, the adhesive tape residue is removed by rinsing the wafer with organic solvents.

Particles of FLBP prepared this way were used to gain valuable fundamental insights on the structure and properties of FLBP and phosphorene.[55–57] However, the mechanical exfoliation method has several serious limitations. First, its low scalability makes it difficult to obtain large quantities of the material, which precludes its use in electronic devices, catalytic systems and biomaterials. Furthermore, due to its unprotected surface, this material is highly susceptible to oxidation in air.[58]

4.1.2. Liquid-phase exfoliation

Liquid-phase exfoliation is the most common method for producing nanoscale BP particles such as few-layer samples and quantum dots. This method produces suspensions of exfoliated BP in various organic solvents. The most suitable solvents for liquid-phase exfoliation of BP are high viscosity polar organic solvents such as *N*-methylpyrrolidone (NMP), DMF, DMSO and ionic liquids.[8,59] It has been shown that due to the adsorption of solvent molecules on the surface of the material, the FLBP obtained by liquid-phase exfoliation has higher oxidative stability compared to mechanically exfoliated FLBP.[60] In addition, the liquid-phase exfoliation method also provides an access to FLBP suspensions in large volumes and with high concentrations (up to 1 mg mL^{-1} when using ionic liquids as a solvent).[59] Pure FLBP can be isolated by centrifuging the suspension at high speeds, washing the precipitate with various volatile solvents, and drying the material *in vacuo*. In practice, several methods are used to obtain FLBP, including sonication- or shear-assisted exfoliation of the FLBP, wet-jet milling, microwave-assisted and electrochemical exfoliation.

Sonication-assisted exfoliation. Currently, sonication-assisted exfoliation of BP is the most common method for producing FLBP. It involves preparing a BP suspension in an organic solvent (usually nmP, DMF, or DMSO) followed by sonication (Fig. 3). Sonication weakens the van der Waals interactions between the BP layers, facilitating their exfoliation. Furthermore, ultrasonic waves create cavitation bubbles between the layers, which, upon collapse, release significant energy, leading to material exfoliation.[61] The key benefits of this technique are its simplicity and the ability to scale up to an industrial scale. Disadvantages include the long exfoliation times (up to 100 h), the relatively low yield of FLBP, and the potential damage to the intralayer P–P bonds under harsh sonication, which leads to a reduction in particle size and a decline in quality of the resulting nanomaterial.

Shear-assisted exfoliation. The shear-assisted exfoliation method was first developed by Coleman and co-workers[62] for the large-scale production of graphene nanosheets. This approach was subsequently successfully adapted for the synthesis of other two-dimensional materials, including FLBP.[8,61,63,64] In particular, Woomer *et al*.[8] demonstrated the possibility of producing FLBP in quantities up to 10 g using this technique. During the experiment, BP crystals were pre-ground in a mortar and dispersed in nmP, after which the resulting suspension was processed in a shear mixer. The mixer design included a four-blade rotor positioned in close proximity (0.2 mm) to a stationary stator. The high rotor speed and minimal gap between the working elements created significant shear stresses, providing effective material exfoliation.

It should be noted that a household kitchen blender can also be used for the BP exfoliation. Xu *et al*.[63] compared the two methods and showed that the quality of BP obtained using a kitchen blender was comparable to that of particles obtained using a laboratory shear mixer.

Wet-jet milling. Wet-jet milling is a method of homogenizing and pulverizing materials that has been widely used in recent years in the ceramic, pharmaceutical and food industries.[65,66] The research group of Del Rio Castillo[66,67] proposed this approach for the exfoliation of various layered materials: graphite, hexagonal boron nitride, transition metal dichalcogenides and BP. In this case, the exfoliation occurs under the influence of shear forces generated by forcing a material suspension under high pressure through narrow (0.1–0.3 mm) orifices. This method enables the rapid and effective production of two-dimensional material suspensions on an industrial scale.

Microwave-assisted exfoliation. Microwave-assisted exfoliation of BP was developed by the Shapter's research group[68] and is one effective method for producing FLBP. The method involves heating a BP suspension in nmP to 50°C, followed by short-term (4–20 min) microwave irradiation. Exposure to microwave irradiation weakens the van der Waals interactions between the BP layers, promoting its exfoliation. The unexfoliated material is then removed by centrifugation. In a follow-up study,[69] it was demonstrated that increasing the suspension temperature and increasing the irradiation duration yields BP quantum dots.

Electrochemical exfoliation. Electrochemical exfoliation is one of the most promising methods for producing FLBP.[70–76] In this case, crystalline BP is used as a cathode together with a platinum anode in a solution of tetraalkylammonium salts in polar organic solvents (DMSO, DMF, propylene carbonate, *etc*.). When high cathodic potentials are applied,

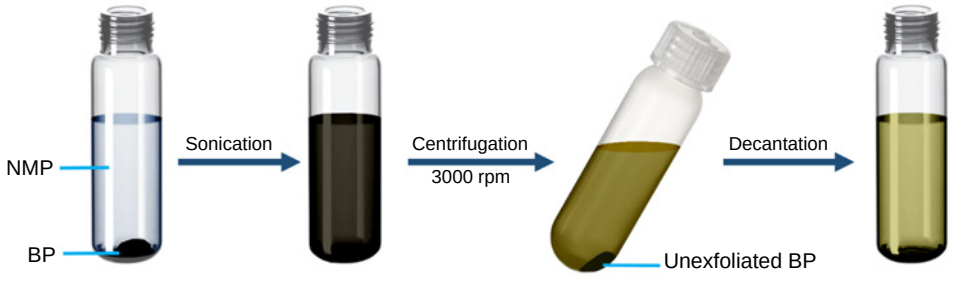

Figure 3. Scheme of sonication-assisted liquid-phase exfoliation of black phosphorus.[24] Reproduced from Kuchkaev *et al*.[24] with the permission from Wiley.

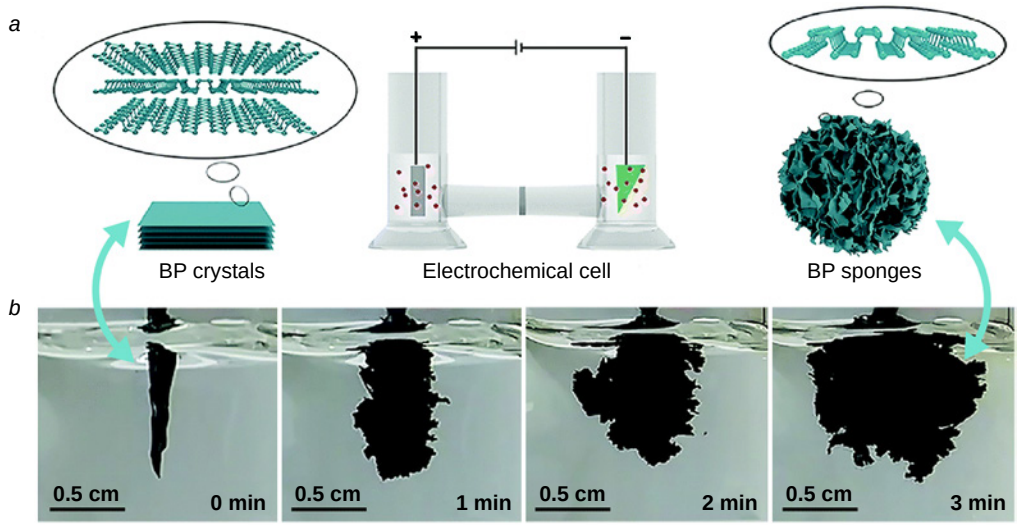

Figure 4. Schematic illustration of electrochemical exfoliation of black phosphorus (*a*), images of the pristine sample and images taken after in 1, 2 and 3 min after voltage was applied (*b*). The Figure was created by the authors using the data of Ref. 77 and published under a CC BY-NC 3.0 license from the Royal Society of Chemistry.

tetraalkylammonium ions intercalate between the FLBP layers, followed by electrochemical reduction of the solvent and electrolyte with the release of gaseous products (Fig. 4). The expansion of these gases leads to exfoliation of the BP layers, forming BP sponges.[74,77] The main advantages of this method are high product yield (>80%) and process speed (a few minutes). Studies by Li *et al.*[74] showed that the highest exfoliation efficiency is achieved using tetrabutylammonium salts, while tetramethylammonium salts exhibit low efficiency due to the formation of bulk solvation shells that hamper intercalation.

Efficient electrochemical exfoliation can also be achieved using BP as the anode.[70,73,78] For example, Shaijumon and co-workers[73] obtained phosphorene quantum dots by anodic exfoliation of BP in propylene carbonate using $LiClO_4$ as the electrolyte. It should be noted that replacing the solvent with formamide resulted in nitrogen-doped BP quantum dots due to the formation of nitrogen-containing charged species during anodic decomposition of the solvent on the BP surface.

Although both methods of electrochemical exfoliation of BP are fundamentally possible, the cathodic exfoliation method is currently more widely used to produce FLBP. This is because anodic reactions on BP promote undesirable oxidative processes during sample exfoliation. Therefore, the cathodic approach yields higher-quality material with fewer structural defects.[76,79]

4.2. 'Bottom-up' methods

The main methods for producing two-dimensional materials using the bottom-up approach are chemical vapour deposition (CVD) and epitaxial growth. These methods are widely used to produce various high-quality 2D materials with large particle sizes.[80–84] Some successful similar approaches have been reported for phosphorene and FLBP.[85,86]

A CVD technique for producing FLBP was developed by Ji and co-workers.[85] First, the authors grew thin films of red phosphorus on a silicon wafer by heating red or black phosphorus powder to 600°C in a tubular furnace. The red phosphorus film was then converted into FLBP by heating the sample to 950°C at a pressure of 27.2 MPa in the presence of Sn/SnI_4 as a mineralizing agent. The resulting FLBP sheets had an average thickness of 2 nm and an area >3 μm^2.

Xu *et al.*[86] used molecular beam epitaxy to produce BP quantum dots anchored on the surface of a silicon wafer. The phosphorus source in this case was white phosphorus, which was transformed into the gas phase at high temperature (900°C). The BP quantum dots were formed by the transfer and deposition of gaseous white phosphorus onto the wafer surface. The resulting particles had a pyramidal structure with an average radius of 27.5 nm and a height of 3.1 nm.

Alternative approaches include solvothermal and mechanochemical methods for the synthesis of FLBP.[87,88] For example, the Tian's research group[87] developed a solvothermal approach to the synthesis of partially oxidized FLBP, which consists of heating a mixture of white phosphorus in ethylenediamine at 60–140°C for 12 h. Park and Sohn[88] proposed an effective method for fabricating FLBP by high-energy mechanical milling of red phosphorus in a ball mill for 54 h. In this case, the conversion of red phosphorus to FLBP was achieved through the formation of local points with high pressure (up to 6 GPa) and temperature (up to 200°C) upon collision of milling bodies.

Although several successful examples of producing FLBP using these methods have been described, the 'bottom-up' approach still requires additional research aimed at increasing scalability and improving the quality of the resulting nanomaterials.

5. Chemical modification of few-layer black phosphorus surface

Despite some unique properties of FLBP, one of the main hurdles of the implementation of materials based on them in modern micro- and optoelectronic devices is their high sensitivity to oxygen and atmospheric moisture. Therefore, methods for protecting the material's surface from oxidation are currently being developed, based on chemical modification of its structure. In many cases, such modifications not only lead to increased stability but can also facilitate the acquisition of new, practically useful properties by the material.[22,24,89] Chemical functionalization of FLBP can be categorized into two main groups, covalent and non-covalent.

Non-covalent functionalization is accomplished through the formation of van der Waals or electrostatic interactions between FLBP and the modifying agent upon its adsorption on the material surface. Classic examples of such interactions include the functionalization of FLBP with surfactants and polymers, which can be used to create stable aqueous suspensions of the

material.[90–93] Stabilization of FLBP occurs through the adsorption of surfactants on the material surface, which creates steric and electrostatic barriers that prevent the aggregation of individual particles.[94] In addition, this method allows the intrinsic structure and electronic properties of FLBP to be preserved due to a significant improvement in the material's oxidation resistance.[90]

During covalent functionalization, the interaction between FLBP and the modifying agent leads to the formation of a phosphorus–element covalent bond. The reactivity of FLBP towards various organic substrates is being actively studied in this area. Highly reactive intermediates have been shown to be the most effective agents.[24] To date, approaches have been developed to functionalize FLBP with aryl radicals during the decomposition of the corresponding diazonium or iodonium salts,[19,95–98] free alkyl radicals,[75,99] carbenes[100] and nitrenes.[101,102] In many cases, the resulting materials demonstrated higher oxidation stability and also exhibited improved electronic, photophysical and catalytic properties.

In addition to functionalization with organic substrates, approaches to modifying the FLBP surface with inorganic functional groups have also been developed. For example, a method for functionalization with OH groups by grinding a mixture of BP and LiOH in a ball mill was developed.[103] Similarly, NH_2-functionalized FLBP were prepared using urea as a reagent.[104] Zhang *et al*.[78] proposed an electrochemical method for producing fluorinated FLBP by anodic exfoliation of BP in the presence of an ionic liquid, a solution of 1-ethyl-3-methylimidazolium tetrafluoroborate (EMIM) in acetonitrile, which acted simultaneously as an electrolyte and a source of fluorine.

Due to its high surface energy and relatively easy functionalization, FLBP is an excellent starting material for modification with various metal substrates.[24] Most often, such systems are 0D/2D nanohybrids, in which two-dimensional FLBP layers act as a carrier for nanoparticles (NPs) of metals, their oxides, or salts. In addition, successful examples of modifying FLBP with individual metal-containing fragments, namely, single atoms, complexes, and subnanometer clusters, are known. The main synthetic approaches to such nanocomposites, as well as their application in various catalytic processes, are discussed in more detail in this and subsequent Sections.

5.1. Modification with transition metal nanoparticles

5.1.1. Deposition of metal nanoparticles by chemical reduction

Over the past several decades, research into nanoscale particles of various compositions has rapidly developed, finding applications in many fields of science, medicine and industry.[105–108] The creation of 0D/2D heterostructures by immobilizing NPs on the carrier surface improves the particles' resistance to aggregation and preserves their fundamental properties. The most common method of immobilization is the simple mixing of suspensions of the carrier and NPs, although in some cases functionalized components are used to increase the stability of the resulting nanocomposite.[94]

Transition metal nanoparticles (TMNPs) are typically prepared by reduction of the corresponding salts.[94] The salt reduction in the presence of a support provides the simultaneous formation and immobilization of metal NPs on the surface of the material. These traditional methods for creating 0D/2D nanocomposites have been widely used to obtain FLBP-supported TMNPs (Fig. 5).[109–116]

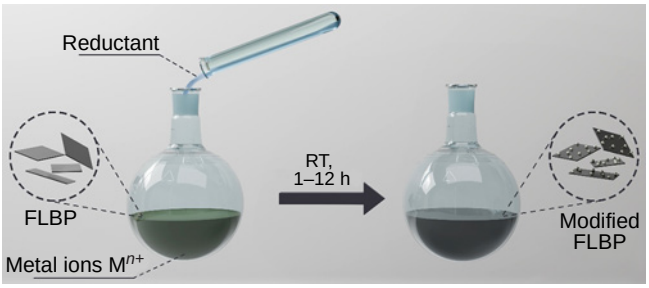

Figure 5. Schematic illustration of modification of few-layer black phosphorus by *in situ* chemical reduction of metal ions. RT is room temperature.

Chen *et al*.[113] synthesized FLBP-supported Pt, Au, and Ag NPs *via in situ* chemical reduction and immobilization technique. The method involved mixing aqueous solutions of the corresponding salts ($PtCl_4$, $HAuCl_4$ or $AgNO_3$) with a suspension of FLBP in NMP and adding a reducing agent, $NaBH_4$, to the resulting mixture. X-Ray photoelectron spectroscopy (XPS) studies of the nanocomposites revealed $P2p_{3/2}/2p_{1/2}$ peaks slightly shifted to higher energies in the spectra, indicating electron density transfer from the FLBP phosphorus atoms to the NPs. Quantum-chemical calculations confirmed this phenomenon. This interfacial charge transfer from the BP surface to supported metals can be used to tune the electronic properties of the resulting composites by changing the nature, structure and composition of the metal NPs. Similar effects were observed in the case of palladium NPs supported on the FLBP surface through the *in situ* reduction of $Na_2[PdCl_4]$ with potassium borohydride.[117]

Liu *et al*.[112] used a similar approach to obtain FLBP-supported PtRu nanoclusters of varying compositions. The resulting nanocomposites were used as catalysts for the electrocatalytic hydrogen evolution reaction. $Pt_1Ru_{1.54}$ nanoclusters exhibited superior activity in the studied process, outperforming a conventional Pt/C catalyst.

Caporali *et al*.[110] immobilized nickel NPs on the FLBP surface by adding their colloidal solution in toluene to a suspension of exfoliated FLBP in THF under vigorous stirring. The resulting material was used as a catalyst in the hydrogenation of phenylacetylene to styrene. This catalyst exhibited high activity, good selectivity, and excellent reusability in the reaction. Furthermore, it was shown that immobilization of nickel NPs increases the oxidation stability of the FLBP under ambient conditions, which can be used in the development of electrochemical gas sensors.[111,118]

The same research group[115] successfully deposited palladium NPs on the FLBP surface by reducing $Pd(NO_3)_2$ with molecular hydrogen in the presence of FLBP. For this purpose, a suspension of the FLBP in THF was mixed with an aqueous ethanol solution of palladium nitrate in an autoclave. The reduction was carried out at a hydrogen pressure of 5 bar at room temperature for 1 h. Using a combination of physicochemical methods, the authors found that this process produced spherical Pd NPs with an average size of 3.1 nm, uniformly dispersed over the FLBP surface. The palladium content in the resulting nanocomposite was 10.6 wt.%.

Mild reducing agents, such as citrate ions, can be used to modify the FLBP surface with gold. For example, Qi and co-

workers[119] successfully immobilized Au NPs on the FLBP surface by reducing $HAuCl_4$ with sodium citrate in an aqueous medium. For this purpose, the reagents were mixed with the suspension of FLBP and the mixture was heated to 100°C with constant stirring for 20 minutes. Using transmission electron microscopy (TEM), a uniform distribution of 12–20 nm gold NPs over the FLBP surface was established. In addition, the polycrystalline structure of the synthesized gold NPs was revealed using selected area diffraction analysis.

Transition metal nanoparticles can also be formed by reducing metal salts with phosphorus atoms on the FLBP surface under UV irradiation or ultrasonication. Warren and co-workers[120] used a photochemical reduction to prepare Au NPs immobilized on the surface of FLBP based on a suspension of FLBP in NMP containing triethylamine and the $[AuCl(PPh_3)]$ complex. Irradiation with 465 nm light initiated the photocatalytic process. Due to its semiconducting properties, the FLBP absorbs photons, leading to the generation of electron-hole pairs. Photoexcited electrons in the conduction band of FLBP reduce the Au^{III} complex to metallic gold(0) on its surface. The resulting holes in the valence band participate in the oxidation of triethylamine, which in this case acts as an auxiliary electron donor.

Later, Xue *et al.*[121] applied a similar approach to immobilize Pt nanoparticles on FLBP under visible light irradiation (λ = 450 nm) in the presence of the sensitizer erythrosine B and triethanolamine, which acted as an electron donor. The authors showed that the resulting system can be used as a highly efficient catalyst for the photochemical hydrogen evolution reaction.

In some cases, FLBP directly acts as a reducing agent for the production of Ag, Au, Pd and Pt NPs.[122–126] Wang and co-workers[124] prepared a composite with FLBP-supported Au NPs by simply mixing aqueous dispersions of FLBP and $HAuCl_4$ and stirring the resulting mixture for several hours. In this case, Au NPs are uniformly distributed over the FLBP surface, and their size largely depends on the FLBP : $HAuCl_4$ ratio used. Thus, a relatively low Au content led to the formation of small (~4 nm) particles, while a high Au content promoted aggregation and led to the formation of larger (~10 nm) NPs. A similar approach was implemented by Veselý *et al.*[125] to obtain an Au NP/MSP nanocomposite in non-aqueous solutions.

Bolognesi and co-workers[127] managed to monitor the formation of gold nanoparticles on the surface of phosphorene. During the study, the authors immersed a substrate with mechanically exfoliated phosphorene in a $[(Me_2S)AuCl]$ solution in chloroform for various periods of time, from 3 to 72 h. More prolonged process was accompanied by a progressive increase in the Au NP size from 10 to 100 nm. The authors also note that partial charge transfer to the Au NPs is observed in the resulting nanocomposites, with positive charge localized on gold atoms directly bonded to the phosphorus atoms of phosphorene. In addition, quantum chemical calculations showed that increasing the gold NP size in the nanocomposite leads to a decrease in the band gap to 1.4 eV, which is 0.8 eV smaller than that of the unmodified material.

Professor Bai and co-workers[128] showed the feasibility of using FLBP for the highly efficient recovery of Pd^{II} and Pt^{II} ions from spent catalysts, producing the corresponding 0D/2D nanocomposites. To extract the noble metals, the authors mixed FLBP with a model solution containing Pd^{II} and Pt^{II} ions in an acidic medium (HCl or HNO_3, pH 1.5). Optimization of experimental conditions enabled Pd extraction efficiencies of up to 99.36% and Pt extraction efficiencies of up to 95.11%. The recovered metals formed nanoparticles directly on the FLBP surface, eliminating the need for additional processing. The resulting nanocomposites were used as catalysts for the hydrogen evolution reaction, where they demonstrated high activity and long-term stability. This approach thus combines efficient extraction of noble metals with direct synthesis of highly active catalysts, offering new solutions for the rational use of resources.

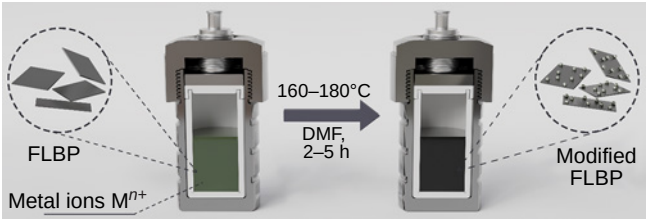

Figure 6. Schematic illustration of modification of few-layer black phosphorus using solvothermal approach.

5.1.2. Solvothermal approaches to the synthesis of 0D/2D nanocomposites

Modification of FLBP with TMNPs can be accomplished using a solvothermal approach. This process is carried out in sealed autoclaves at temperatures above the boiling point of the solvent, which enhances the reactivity of the reagents and solvent used, delivering materials with diverse structures. In particular, this method gave rise to FLBP-based nanocomposites with TMNPs immobilized on the material's surface, as well as their phosphides (Fig. 6). It should be noted that in most cases, solvothermal synthesis was carried out in DMF or oleylamine, which exhibit pronounced reducing properties at elevated temperatures.[129–131] Therefore, in the cited studies, the solvent served as the reducing agent for the metal precursors.

Professor Feng and co-workers[114] presented an approach to the solvothermal synthesis of the FLBP-supported Co NPs. For this purpose, a suspension of FLBP was prepared in oleylamine in the presence of cobalt(II) nitrate. The reaction was carried out at 245°C for 1 h. Using high-resolution TEM and selected area electron diffraction, the authors showed a uniform distribution of cobalt NPs with an average size of 21 nm over the surface of the FLBP. Furthermore, a detailed analysis of the XPS spectra revealed that electron density transfer from phosphorus atoms to cobalt atoms is observed in this nanocomposite at the interface between FLBP and the Co NPs. The absence of signals of the Co–P bond indicates immobilization of Co NPs on the FLBP surface *via* van der Waals interactions. Further study of the optical and electrochemical properties of the resulting material revealed a decrease in the band gap and an increase in the electrical conductivity of the Co/FLBP composite, enabling its use as a catalyst in the electrochemical oxygen evolution reaction.

Li *et al.*[132] used a solvothermal approach to modify FLBP with bimetallic palladium and copper NPs. The authors used copper(II) and palladium(II) acetates as precursors, and the synthesis was carried out in DMF at 160°C for 4 h. Using various physicochemical methods, it was shown that this process affords amorphous PdCu NPs with an average size of 10 nm on the FLBP surface. XPS data indicated that the metals were predominantly in the 0 oxidation state, with electron density transfer observed from the FLBP phosphorus atoms to the metal centres. Modification of the PdCu NPs increased the oxidation stability of the FLBP under conditions of electrochemical oxygen reduction and hydrogen evolution reactions.

One of the key features of the solvothermal method for modifying FLBP is the ability to functionalize the its surface with transition metal phosphides.[133–137] It has been shown that this modification of FLBP opens the way to materials with increased resistance to environmental conditions, as well as improved optical and electrochemical properties. The resulting composites find application as sensors and catalysts for various processes.[134,137–140] In most cases, FLBP act as a substrate and source of phosphorus during the formation of metal phosphides.

Yan and co-workers[133] prepared a Ni_2P/FLBP composite *via* a solvothermal reaction using $NiCl_2$ in the presence of FLBP in DMF. Heating the resulting mixture to 160°C in an autoclave gave uniformly distributed Ni_2P NPs with a diameter of 5 nm on the FLBP surface. Further experiments showed that the Ni_2P/FLBP composite exhibited enhanced conductivity due to an increased charge carrier concentration and reduced thermal conductivity at 300 K compared to the starting sample. These properties made it possible to use the resulting material as an anode in lithium-ion batteries, as well as an effective electrocatalyst for hydrogen evolution reaction. The excellent activity of Ni_2P/FLBP in the hydrogen evolution reaction was also demonstrated by Lin *et al.*[134] It should be noted that varying the concentration of $NiCl_2$ during solvothermal synthesis affords Ni_2P/FLBP nanocomposites with different Ni : P ratios.[140]

The solvothermal method is also widely used to prepare heterostructures of cobalt phosphides and FLBP.[135–139,141] Liang *et al.*[135] synthesized a CoP/FLBP nanocomposite, as described above for Ni_2P/FLBP, using $CoCl_2$ as the metal precursor. In this case, CoP NPs with an average diameter of 5 nm were uniformly distributed over the surface of the material. Strong interactions between CoP and FLBP promote rapid charge transfer and reduce charge recombination in the CoP/FLBP hybrid, which enhances the photocatalytic activity of the material.

Yang *et al.*[138] developed a new method for the synthesis of two-dimensional transition metal phosphides by doping BP layers using a solvothermal approach. During the synthesis, Co^{II} or Ni^{II} acetylacetonate was mixed with a suspension of electrochemically exfoliated BP in DMF. The mixture was then heated at 180°C for 5 h in a Teflon-lined autoclave to deliver two-dimensional transition metal phosphides Co_2P and $Ni_{12}P_5$. Furthermore, the authors demonstrated the feasibility of synthesizing bimetallic phosphides $Co_xFe_{2-x}P$ $(0 < x < 2)$ by varying the molar ratios of the starting reagents containing Co, Fe, and P.

The doping mechanism was studied in detail and is presented in Fig. 7 (AFM is atomic force microscopy). According to the proposed scheme, the surface of FLBP interacts with DMF at high temperatures, which is accompanied by the release of phosphine PH_3 and the formation of phosphorus vacancies in the crystal lattice. Phosphorus atoms adjacent to the vacancies continue to react with DMF to form hydrogenated phosphorus moieties. These hydrogenated phosphorus units subsequently reduce metal ions, facilitating their incorporation into the lattice

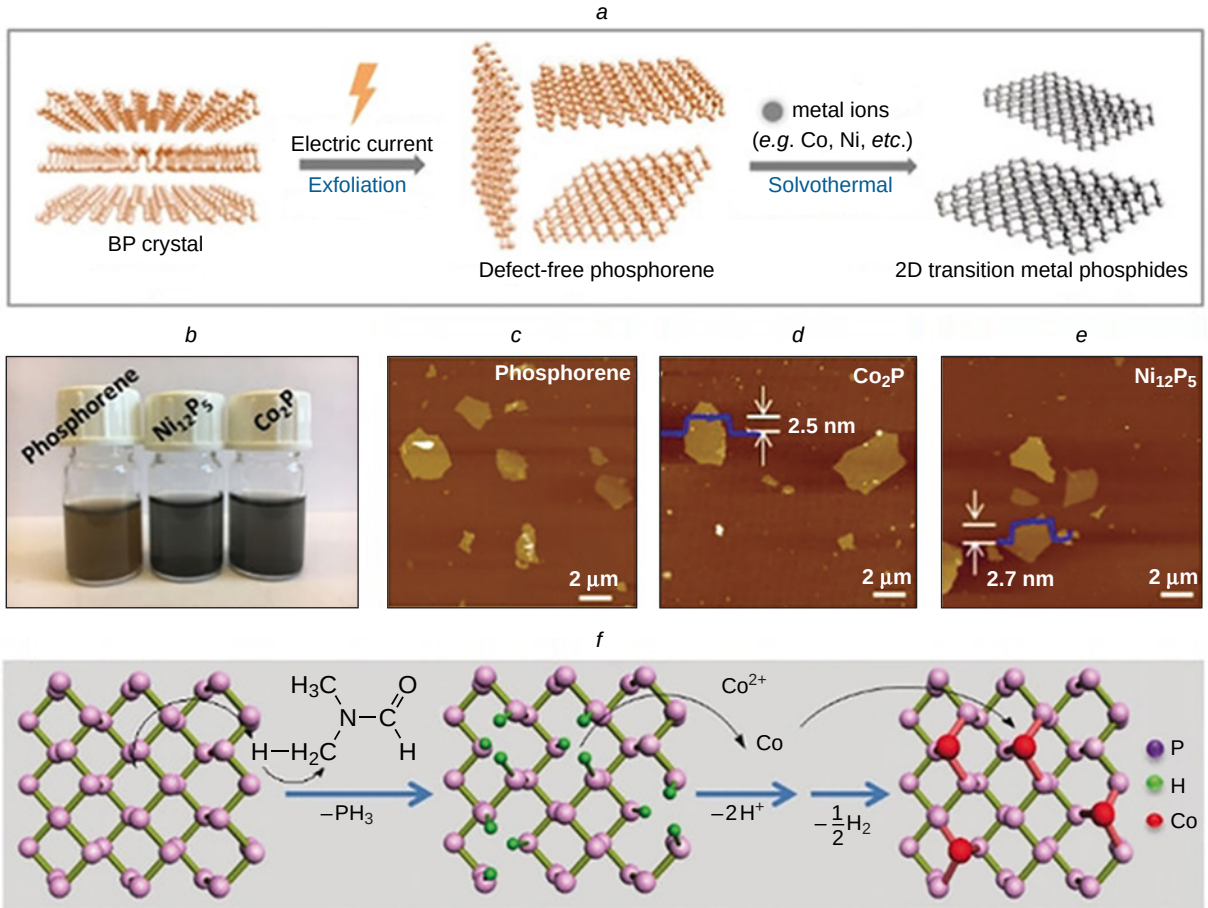

Figure 7. Synthesis of 2D transition metal phosphides (*a*); optical images of 2D phosphide suspensions in DMF (0.2 mg mL^{-1}) (*b*); AFM images of phosphorene (*c*), $Ni_{12}P_5$ (*d*) and Co_2P (*e*); reaction pathway for the synthesis of 2D Co_2P by the solvothermal method (*f*). The Figure was created by the authors based on data of Ref. 138 and reproduced under a CC BY license from Wiley.

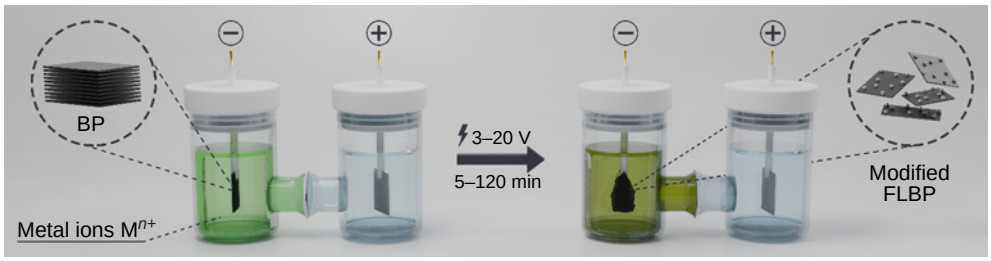

Figure 8. Electrochemical modification of few-layer black phosphorus.

and the formation of two-dimensional phosphides. The resulting two-dimensional materials are noted to possess p-type semiconductor properties. Furthermore, $Co_{1.5}Fe_{0.5}P$ species shows high catalytic performance and good stability in the electrochemical oxygen evolution reaction.

5.1.3. Electrochemical modification with transition metal nanoparticles

In recent years, electrochemical approaches to modifying FLBP with inorganic substrates have been actively developed. These methods are based on cathodic electrochemical exfoliation of FLBP in the presence of transition metal salts, enabling the *in situ* production of FLBP modified with reduced forms of metal precursors (Fig. 8). For example, Kovalska *et al.*[142] carried out cathodic electrochemical exfoliation of BP in the presence of various platinum group salts: $RuCl_3$, $RhCl_3$ and $PdCl_2$. The electrochemical exfoliation and reduction were carried out in DMF in the presence of a 0.01 M solution of tetrabutylammonium hexafluorophosphate (Bu_4NPF_6) and a 0.03 M solution of metal chloride at an applied potential of –3.8 V. TEM images of the resulting nanocomposites revealed the formation of metal NPs on the surface of the exfoliated BP sheets. The mass content of NPs on the BP surface increased in the order Ru < Rh < Pd and amounted to 0.5, 1.4 and 9.2 wt.%, respectively. Palladium and rhodium salts proved to be more suitable reagents for this process than ruthenium chloride and furnished uniformly distributed round NPs with a diameter of 2–5 nm on the FLBP surface. Finally, the authors showed that deposition of platinum group metal NPs on FLBP increases the electrochemically active area, conductivity and other electrochemical characteristics of the material, which can find application in various sensor devices, electrochemical catalysts and batteries.

Yang and co-workers[139] developed an electrolysis-solvothermal method for producing a CoP/FLBP nanocomposite (Fig. 9). In the experiment, cathodic exfoliation of BP was performed using a Co wire as a soluble anode and a cobalt source. Applying a voltage between the BP cathode and the cobalt anode induced exfoliation of BP along with the oxidation of metallic Co and the formation of Co^{2+} ions in solution. After electrolysis, the mixture was transferred to an autoclave and subjected to solvothermal treatment at 160°C to produce the CoP/FLBP nanocomposite. Immobilization of CoP NPs significantly improved the oxidative stability of FLBP in air, preventing their degradation. Using a cobalt wire as a soluble anode also resulted in the formation of less oxidized FLBP during electrochemical exfoliation. In addition to surface stabilization, CoP NPs also enhanced the material's catalytic activity in the electrochemical oxygen evolution reaction.

Xiao *et al.*[143] used an electrochemical approach to obtain FLBP with Pd nanoclusters intercalated between the BP layers. For this purpose, cathodic exfoliation of BP was carried out in DMSO in the presence of $PdCl_2$ and tetrabutylammonium

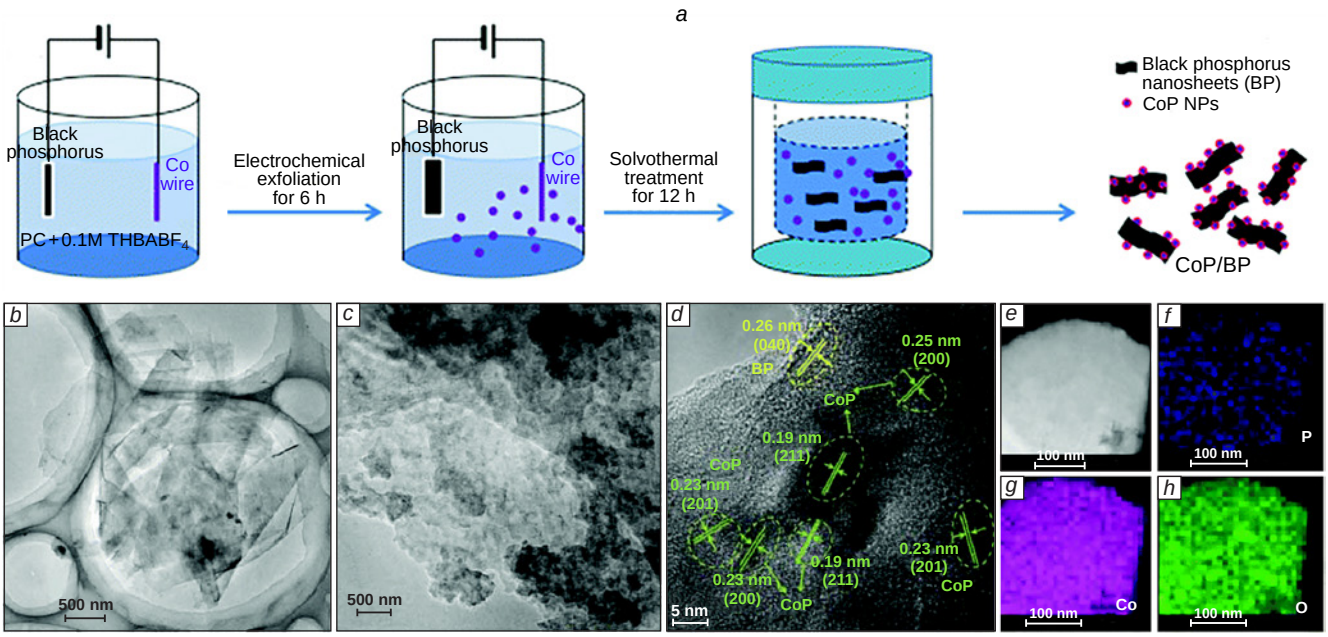

Figure 9. Schematic for the electrolysis-solvothermal synthesis of CoP/FLBP (*a*); TEM images of CoP/FLBP of different scale (*b*, *c*) and high-resolution TEM image (*d*); TEM image of CoP/FLBP particles (*e*) Elemental mapping of the corresponding area (*f*–*h*). The Figure was adapted from Ref. 139 and published under a CC BY-NC 3.0 license from the Royal Society of Chemistry.

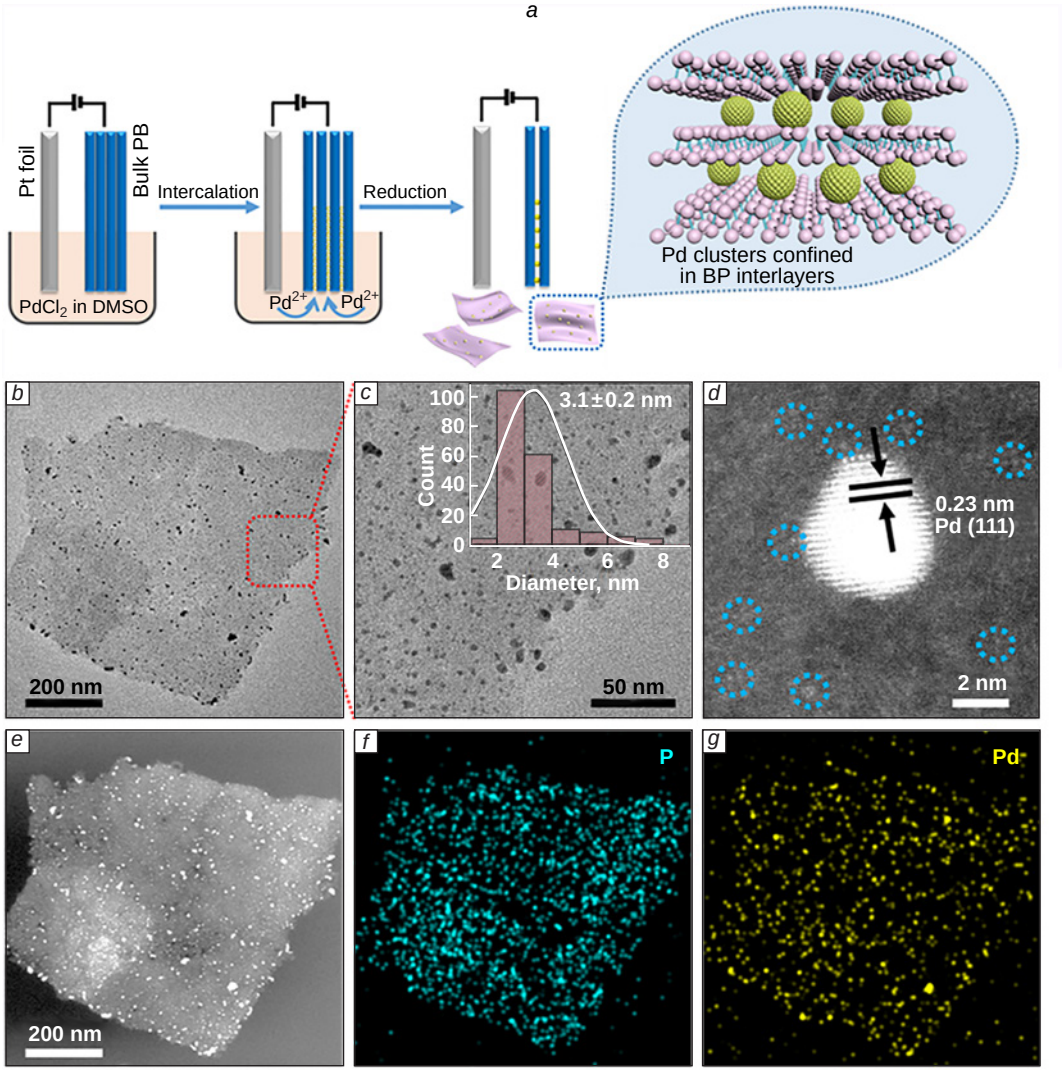

Figure 10. Electrochemical intercalation of Pd nanoclusters between the FLBP layers (*a*); TEM images of Pd-i-BP particles on a different scale (*b*, *c*); aberration-corrected HAADF-STEM image of Pd-i-BP species (single atoms or small Pd clusters are marked with light blue circles) (*d*); STEM images of Pd-i-BP particles (*e*) and EDS mappings (*f*, *g*) of the corresponding areas.[143] Published under a CC BY-NC 4.0 license from AAAS.

hydroxide (Bu_4NOH) as a background electrolyte (Fig. 10).[†] Electrolysis was carried out at a potential of –2.0 V for 1 h. Using *in situ* electrochemical TEM, the authors were able to monitor the intercalation and reduction of Pd ions between the BP layers in real time. The experiments revealed that the intercalation of Pd^{2+} ions increases the interlayer spacing of BP. This process is accompanied by the reduction of intercalated palladium ions to Pd atomic species, which then assemble into nanoclusters within the BP layers. The growth of Pd nanoclusters weakens the van der Waals interactions between the BP layers, leading to their delamination. In addition to TEM, the formation of intercalated Pd particles was also confirmed by X-ray powder diffraction (XRPD), as evidenced by a shift in the peak of the (020) crystal plane from 16.9° to 16.7°, indicating a change in the interlayer spacing. In addition, according to the XPS data, the ratio of integrated signal intensities related to P and Pd atoms remains constant throughout the entire depth of the material, demonstrating the uniform distribution of palladium particles during their intercalation and reduction. Finally, the authors demonstrated that the developed method for modifying FLBP can be applied to the production of Ag/FLBP and Rh/FLBP nanocomposites.

An interesting feature of the electrochemical modification of FLBP is the ability to use the anode material to generate transition metal cations in solution, which participate in surface modification. For example, Professor Yang and co-workers[144] carried out cathodic exfoliation of BP using a nickel-cobalt anode. The anodic reaction in this case involves the dissolution of the anode, forming Ni^{2+} and Co^{2+} ions, which are then transferred to the cathode material and reduced to form metallic nanoparticles. It should be noted that electrochemical exfoliation or modification of BP using a Ni and Co anode sequentially allows for the production of a BP with nickel and cobalt NPs co-loaded onto its surface.

Table 1 presents the main approaches to modifying FLBP with transition metal nanoparticles.

[†] Pd-i-BP means Pd cluster–intercalated black phosphorus; HAADF-STEM is high-angle annular dark-field scanning transmission electron microscopy.

Table 1. Modification of few-layer black phosphorus with transition metal nanoparticles.

Nanocomposite	Modification method	Application	Ref.
Pt, Au, Ag – FLBP	*In situ* chemical reduction	Electrocatalytic oxygen reduction	113
Pd/FLBP	*In situ* chemical reduction	Catalytic hydrogenation of 4-nitrophenol	117
PtRu/FLBP	*In situ* chemical reduction	Electrocatalytic hydrogen evolution	112
Ni/FLBP	Mixing suspensions of FLBP and metal NPs	Catalytic hydrogenation of phenylacetylene	110
Ni/FLBP	*In situ* chemical reduction Mixing suspensions of FLBP and metal NPs	Electrochemical NO_2 sensors	118
Pd/FLBP	*In situ* chemical reduction	Catalytic hydrogenation of chloronitroarenes	115
Au/FLBP	*In situ* chemical reduction	Electrocatalytic oxygen evolution	119
Au/FLBP	Photochemical reduction of metal salts on the FLBP surface	Photocatalytic hydrogen evolution	120
Pt/FLBP	Photochemical reduction of metal salts on the FLBP surface	Photocatalytic hydrogen evolution	121
Au/FLBP	Reduction of FLBP metal precursors	Catalytic reduction of nitro compounds	124
Au/FLBP	Reduction of FLBP metal precursors	Catalytic oxidation of acrylic acid	125
Au/FLBP	Reduction of FLBP metal precursors	–	127
Pd, Pt – FLBP	Reduction of FLBP metal precursors	Photocatalytic hydrogen evolution	128
Co/FLBP	Solvothermal synthesis	Electrocatalytic oxygen evolution	114
PdCu/FLBP	Solvothermal synthesis	Electrocatalytic oxygen reduction and hydrogen evolution	132
Ni_2P/FLBP	Solvothermal synthesis	Electrocatalytic hydrogen evolution	133, 134
Ni_2P/FLBP	Solvothermal synthesis	Electrochemical L-cysteine sensor	140
CoP/FLBP	Solvothermal synthesis	Photocatalytic hydrogen evolution	135
CoP/FLBP	Electrolysis-solvothermal synthesis	Electrocatalytic oxygen evolution	139
Co_2P, $Ni_{12}P_5$, $Co_xFe_{2-x}P$	Solvothermal synthesis	Electrocatalytic oxygen evolution	138
Ru, Rh, Pd – FLBP	Electrochemical exfoliation of BP in the presence of metal salts	Sensors, electrocatalysts for hydrogen evolution reaction, batteries	142
Pd/FLBP	Electrochemical exfoliation of BP in the presence of metal salts	Electrocatalytic CO_2 reduction	143
Co, Ni – FLBP	Electrochemical exfoliation of BP in the presence of metal salts	Electrocatalytic oxygen evolution	144

5.2. Modification with discrete metal fragments

Transition metal nanoparticle-based materials are widely used in heterogeneous catalysis and are the subject of intensive research in this area. Their catalytic activity is directly related to particle size, with the most active sites typically being the coordinatively unsaturated metal atoms on the edges and surface defects.[145–148] Reducing the NP size allows not only for a significant increase in the specific surface area but also for an increase in the catalyst's specific activity per metal atom due to an increased proportion of such low-coordinated active sites. The logical conclusion of this trend is the transition to single-atom catalysts, where each metal atom, individually anchored to the support surface, acts as an active site. This approach allows for the highest possible efficiency in the use of atoms, which is particularly important for noble metals, and also ensures exceptional selectivity of catalytic processes due to the homogeneity and precise definition of the structure of the catalyst active sites.[149–152] Moreover, since the metal atoms are directly bound to the support surface, its structure and chemical nature directly affect the electronic state of the metal centre, which ultimately determines the catalytic activity and selectivity of the entire system.[152–155] Furthermore, it should be noted that reducing the size of metal nanoparticles to clusters and individual atoms significantly increase their surface energy, which, in turn, facilitates their aggregation into clusters and nanoparticles.[151] Therefore, there is an active search for supports capable of strong interactions with metal atoms, which will help to maintain a high dispersion of metal-containing species on the material surface during catalytic processes. Thus, along with the nature of the metal, the choice of support plays a key role in the design of single-atom catalysts.

Due to the presence of lone electron pairs at the sp^3 hybridized phosphorus atoms, as well as its unique puckered structure, FLBP is considered a highly promising support for the creation of single-atom catalysts based thereon.[156–158] Yang *et al*.[156] used density functional theory (DFT) calculations to systematically study the coordination, stability and electronic properties of 3d- (Fe, Co, Ni, Cu), 4d- (Ru, Rh, Pd, Ag), and 5d-metals (Os, Ir, Pt, Au) adsorbed on a FLBP monolayer. It was shown that adsorption of a metal atom in the hollow site (the centre of a six-membered phosphorus ring), substitution of a phosphorus atom for a metal atom and incorporation into the near surface layer afford the most stable single-atom catalysts. The formation of strong P–metal coordination bonds in the phosphorene molecule prevents metal atom migration and aggregation. Analysis of the electronic properties of the simulated systems revealed a clear relationship between the electronegativity of the metal atoms and the electron density distribution in these systems. Thus, metals with a lower electronegativity compared to phosphorus acquire a partially positive charge, metals with similar electronegativity remain neutral, while more electronegative metal atoms pull electron density towards themselves and acquire a partial negative charge.

It has been shown that doping phosphorene with various elements also allows fine-tuning the electronic properties of metal centres in single-atom catalysts.[157,158] The authors studied the adsorption energies of various small molecules for the most stable configurations. Calculations revealed that a rhodium-

based system (Rh/BP), exhibiting balanced adsorption of CO and O_2, can show high catalytic activity in the CO oxidation reaction.[156] At the same time, similar systems based on nickel (Ni/BP) and palladium (Pd/BP), due to their strong adsorption of molecular hydrogen, can display catalytic activity in the hydrogenation reactions of unsaturated compounds. In addition, Zhong *et al*.[157] used DFT calculations to theoretically analyze 27 different single-atom catalysts based on phosphorene and 3d, 4d, and 5d metals for the electrocatalytic CO_2 reduction reaction. Among these systems, catalysts containing Zr, Nb, and Ru performed best in this process. These studies indicate that the development of single-atom catalysts based on phosphorene and FLBP holds great promise.

When considering synthetic approaches to modifying FLBP with individual metal-containing moieties, it is worth noting the presence of lone electron pairs at the phosphorus atoms. This opens up new possibilities for FLBP functionalization through its coordination to metal atoms in metal complexes and the formation of bonds *via* a donor-acceptor mechanism. For example, the research groups of Rao[159] and Velian[160] developed approaches to modifying the surface of FLBP with Lewis acids. According to the experiments, FLBP behaviour is consistent with the principle of hard and soft acids and bases (HSAB): being a soft base, phosphorus atoms on the surface of the material formed stronger bonds with soft Lewis acids, such as aluminum and gallium halides.[160]

An interesting area of research is the immobilization of transition metal complexes on the FLBP surface. In such nanocomposites, FLBP simultaneously acts as a solid support and a polyphosphorus ligand. DFT calculations performed by Ienco *et al*.[161] demonstrate the fundamental possibility of forming coordination compounds between the phosphorus atoms of phosphorene and certain unsaturated metal complexes *via* the η^1-, η^2- and η^3-type addition (Fig. 11). At the same time, the authors note that in the cases of η^2 and η^3 coordination to metal centres, optimal overlap of molecular orbitals is not observed, which leads to an increase in the lengths of P–metal bonds, distortion of the structure and, accordingly, the formation of less strong bonds compared to those in complexes with molecular phosphines.

The first experimental example of the functionalization of FLBP with transition metal complexes was the work of Zhao *et al*.,[162] in which the titanium *p*-toluenesulfonate complex TiL_4 was used as a reagent. In the resulting material, the LEPs of the phosphorus atoms were involved in the formation of coordination bonds with titanium atoms, significantly improving its oxidation stability. Later, materials based on FLBP modified with sulfonate complexes of ruthenium and several lanthanides were also obtained.[163,164]

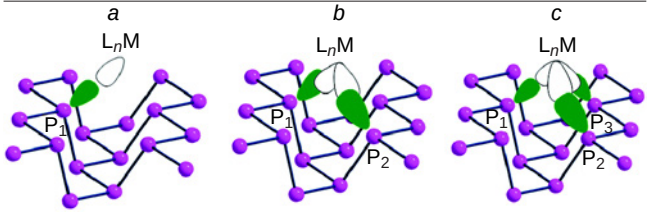

Figure 11. Phosphorene models with differently anchored L_nM complexes: η^1 coordination of the phosphorus atom with a single σ-acceptor metal (*a*); η^2 coordination at a doubly (*cis*) unsaturated metal fragment (*b*); and η^3 coordination at a triply (*fac*) unsaturated metal fragment (*c*).[161] Published under a CC BY 3.0 license from the Royal Society of Chemistry.

In 2023, Professor Velian's research group[165] proposed using rhenium and molybdenum carbonyl complexes $Re(CO)_5Cl$, $CpRe(CO)_3$, $Re(bipy)(CO)_3Cl$ and $[CpMo(CO)_3][BF_4]$, where Cp is cyclopentadienyl and bipy is 2,2′-bipyridine, to functionalize FLBP. The formation of the phosphorus–metal covalent bond, as well as the functionalization of FLBP with individual metal centres, were confirmed by STEM, extended X-ray absorption fine structure (EXAFS), and X-ray absorption near-edge structure (XANES) spectroscopy. Using IR spectroscopy, the authors assessed the steric and electronic properties of FLBP as a ligand and compared the results with those for molecular phosphines. It was found that, in terms of steric properties, FLBP is similar to tri(*p*-tolyl)phosphine in monodentate coordination to metal atoms and to bis(diphenylphosphino)propane in bidentate coordination. At the same time, in terms of its electronic properties, FLBP resembles trialkylphosphines, possessing pronounced σ-donor properties.

Peruzzini and co-workers[166] found that reduction of $[Pd(C_3H_5)Cl]_2$ complex with FLBP results in intercalation of Pd_2 units between the FLBP layers. X-ray powder diffraction, TEM, and IR spectroscopy studies confirmed that the functionalization does not disrupt the FLBP crystal lattice, and that Pd is uniformly distributed in the Pd_2/FLBP bulk without the formation of large nanoparticles or palladium phosphides (Fig. 12). Furthermore, using XPS and EXAFS techniques, it was found that the Pd atoms are in a state close to Pd^0, forming strong Pd–P bonds. The obtained data indicate a strong electronic interaction between Pd and the FLBP in this material.

Chen *et al*.[167] developed a method for modifying FLBP with Pd and Pt atoms using atomic layer deposition. For this purpose, the FLBP particles were preheated to 150°C to remove adsorbed species and to create surface defects that served as additional vacancies for the subsequent anchoring of organometallic precursors – palladium(II) hexafluoroacetylacetonate ($Pd(hfac)_2$) and trimethyl(methylcyclopentadienyl)platinum(IV) ($MeCpPtMe_3$). Subsequent ozone treatment of modified FLBP particles at 150°C removed the organic ligands, yielding pure monatomic centres. The formation of single-atom catalysts was unambiguously confirmed by HAADF-STEM, which visualized isolated metal atoms located in vacancies along the zigzag lattice plane of FLBP. Elemental mapping of the studied samples also confirmed the uniform distribution of the metals.

In-depth studies using XANES and EXAFS techniques revealed the valence state of Pd and Pt atoms in the resulting materials.[167] Thus, the palladium atoms in the Pd_1/FLBP composite are in the zero-valence state, while the platinum atoms in Pt_1/FLBP were more susceptible to oxidation and demonstrated a high oxidation state (+2 or +4), and oxygen atoms were present in their coordination sphere along with phosphorus atoms. Finally, the authors applied the resulting single-atom catalysts to the hydrogenation of phenylacetylene to styrene. It was shown that Pd_1/FLBP showed superior activity and selectivity (up to 99%) in the formation of styrene, while Pt_1/FLBP particles catalyze predominantly exhaustive hydrogenation to ethylbenzene.

Ren *et al*.[168] immobilized individual cobalt atoms on the surface of FLBP by calcining a mixture of FLBP and $CoCl_2$ in an argon flow at 300°C for 2 h. Using modern microscopy techniques, the authors demonstrated a uniform distribution of individual Co atoms over the entire surface of the material. In addition, analysis of XPS, XANES, and EXAFS spectra revealed the formation of a strong Co–P bond in the resulting material in the absence of Co–Co bonds, confirming the monatomic nature

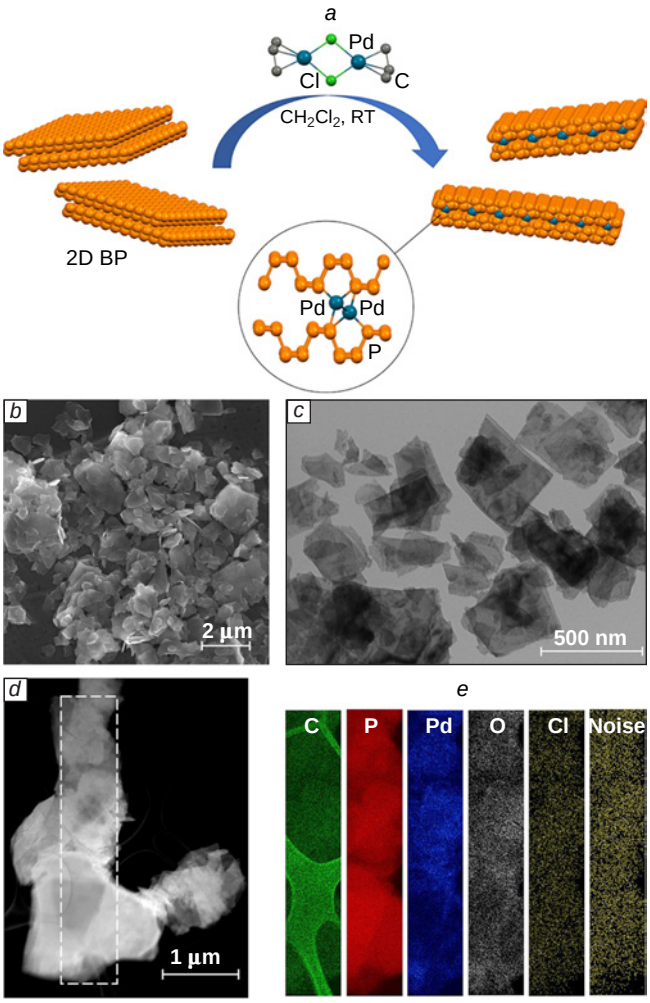

Figure 12. The mechanism of coordination of Pd_2 units between the FLBP layers (*a*); SEM (*b*) and TEM (*c*) images of Pd_2/FLBP particles; HAADF-STEM image of Pd_2/FLBP particles (*d*) with elemental mapping of the region highlighted in *d* (*e*).[166] Published under a CC BY 4.0 license from the American Chemical Society.

of cobalt distribution over the FLBP surface. This modification of FLBP improved the photophysical properties of the material and was used to create photocatalytic systems for hydrogen evolution and CO_2 reduction reactions.

Electrochemical methods for the surface modification of FLBP with metal-containing fragments have also been reported. For instance, Yu and co-workers [169] developed an electrochemical approach to fabricate FLBP doped with Ni, Co, and Mo atoms. Metal precursors included $NiCl_2$, $CoCl_2$ and $MoCl_5$. Electrolysis was performed in an H-cell in DMF in the presence of tetrabutylammonium ions at an applied voltage of 20 V for 3 min. This rapid exfoliation–modification process affords FLBP particles with metal atoms uniformly dispersed over the material surface. Inductively coupled plasma mass spectrometry determined the Ni, Co, and Mo contents in the modified materials to be 1.2, 4.0, and 2.3 wt.%, respectively.

Using cobalt as an example, the authors studied in detail the effect of electrolysis conditions on the structure of the resulting products.[169] In particular, they found that two-step electrolysis with the addition of Co^{2+} ions after preliminary exfoliation of BP produced large nanoparticles on the FLBP surface. Conversely, when carrying out electrolysis without a background electrolyte, colloidal Co particles were deposited on the surface of BP, but without its exfoliation. Thus, the key role of the background electrolyte in the electrochemical exfoliation and modification of BP was established. The authors proposed a mechanism for this process in which, in the first step, tetrabutylammonium ions are inserted between the layers of polarized crystalline BP, which is followed by their reduction to form tributylamine and leads to the expansion of the cathode material. The resulting tributylamine then forms a cationic complex with Co^{2+} ions, which, along with free Bu_4N^+ ions, intercalates between the layers of BP. Being influenced by the cathode's negative charge, the complex is attracted to its surface and reduced to atomic cobalt.

Electrochemical modification can also be used to immobilize bimetallic substrates on the FLBP surface. For example, Zhai *et al.*[170] modified FLBP with Ni_3Pd_1 or Ni_3Fe_1 nanoclusters *via* cathodic exfoliation of BP in the presence of $NiCl_2$ and $PdCl_2$ or $FeCl_2$, taken in a 3 : 1 molar ratio. Using high-resolution TEM and a set of spectroscopic techniques, the authors found that these processes provided a uniform distribution of Ni_3Pd_1 and Ni_3Fe_1 clusters over the entire FLBP surface giving no metallic NPs and aggregates. Moreover, XPS and XRPD data indicate covalent modification of FLBP with the formation of P–Ni and P–Pd (or Fe) bonds. This modification of FLBP improved the material's electrical conductivity and significantly increased its catalytic activity in hydrogen and oxygen evolution reactions.

6. Application of black phosphorus-based materials in catalytic processes

Due to its high specific surface area and charge carrier mobility, as well as its tunable band gap, FLBP is a promising material for the creation of effective catalysts for chemical reactions.[25–27,171,172] For example, electrocatalytic systems based on FLBP modified with various metallic substrates are currently being actively developed. Such modification often improves the material's stability in catalytic processes, increases its electrical conductivity, and creates additional active sites for various electrochemical processes.[25,26] Due to their high susceptibility to oxidation, FLBP-based materials have found widespread use in cathodic (reductive) processes, such as hydrogen evolution and nitrogen fixation. However, there are also successful studies using FLBP in oxidative processes, such as the electrochemical oxygen evolution.

The high negative position of the bottom of the conduction band of FLBP (up to ≈–1.0 V *vs* standard hydrogen electrode (SHE)) [103] provides exceptional reducing power of photoexcited electrons. This makes this material a promising catalyst for photocatalytic reduction processes, including hydrogen evolution reactions, CO_2 reduction, and molecular nitrogen fixation.[27,171] To achieve greater charge separation and improve the efficiency of such processes, the FLBP surface is often modified with transition metal NPs, and heterostructures are created with other semiconductor materials possessing a complementary band structure.[173] Transition metal nanoparticles serve as active centres for electron accumulation, locally concentrating reduction processes on their surface. At the same time, in heterostructures (*e.g.*, in the structure of FLBP, graphite-like carbon nitride (g-C_3N_4)), a spatial charge separation occurs, in which electrons retain high reducing activity in FLBP, and oxidation processes are transferred to the second component. Additional introduction of easily oxidizable reagents into the process, such as triethanolamine or methanol, helps to compensate the moderate oxidation potential of FLBP (≈+0.3 V *vs* UHE),[103] effectively 'diverting' holes to side reactions and

thereby increasing the overall photocatalytic activity of the system.[173]

This Section will discuss the main electro- and photocatalytic FLBP-based systems, designed for the hydrogen and oxygen evolution reactions, CO_2 reduction and nitrogen fixation.

6.1. Hydrogen and oxygen evolution reactions

In the context of the global transition to sustainable development and the implementation of environmentally friendly technologies, considerable attention is being paid to the study of alternative energy sources. Hydrogen is considered one of the most promising candidates for replacing traditional energy sources due to its high energy density, environmental safety and zero emissions during combustion.[173,174] Among state-of-the-art eco-friendly methods for hydrogen production, approaches based on photo- and electrocatalytic water splitting are actively being developed.[175,176] Two-dimensional materials, particularly those based on FLBP, are of great interest for use in these processes. For example, quantum chemical calculations[177] demonstrated the fundamental possibility of using phosphorene and FLBP in photocatalytic water splitting reactions.

However, according to experimental data, the quantum yields of hydrogen (H_2) for the FLBP-based system were low.[159] The low efficiency of such catalysts is due to the high Gibbs energy at the step of formation of the adsorbed hydrogen atom (H*). According to theoretical calculations, the ΔG_{H^*} value for FLBP is ~1.23 eV, which makes the entire proton reduction process energetically unfavourable and leads to the recombination of photoexcited charge carriers.[178] Therefore, various types of surface modification of phosphorene and FLBP are used to improve the efficiency of catalytic systems. For example, FLBP sheets modified with $InCl_3$ and $B(C_6F_5)_3$ moieties showed high efficiency in photocatalytic hydrogen evolution.[159] The hydrogen yields for FLBP/$InCl_3$ and FLBP/$B(C_6F_5)_3$, equal to ~2060 and ~6600 μmol h^{-1} g^{-1}, respectively, exceeded those of many photocatalytic systems based on noble metals and other two-dimensional materials. And functionalization of FLBP with OH groups increased its photocatalytic activity by >18 times, reaching 512 μmol h^{-1} g^{-1}.[103]

High catalytic performance in the photochemical hydrogen evolution was demonstrated by such heterostructures as FLBP/TiO_2, FLBP/g-C_3N_4, FLBP/$BiVO_4$ and FLBP/MoS_2.[179–183] In these cases, it was due to efficient charge separation and inhibition of charge carrier recombination in the materials. For the FLBP/$BiVO_4$ nanocomposite, charge separation occurs according to the Z-scheme: excited electrons from the conduction band of $BiVO_4$ recombine with photogenerated holes in the FLBP valence band.[181] In the FLBP/g-C_3N_4 composite, excited electrons from the conduction band of g-C_3N_4 transfer to FLBP.[179,182]

Caporali and co-workers[183] obtained ternary heterostructures based on TiO_2 modified with FLBP and CoP particles (Fig. 13) in different ratios and studied these materials in the photocatalytic hydrogen evolution. Among the studied systems, the highest activity (7400 μmol h^{-1} g^{-1}) was demonstrated by a catalyst based on TiO_2 containing 1 and 2 wt.% FLBP and CoP, respectively. In this composite, excited electrons from the FLBP and TiO_2 are transferred to the CoP NPs, which leads to efficient separation of photoexcited charges in space and an increase in catalytic activity.

Table 2 systematizes the literature data on the efficiency of various FLBP-based materials in the photocatalytic hydrogen evolution reaction.

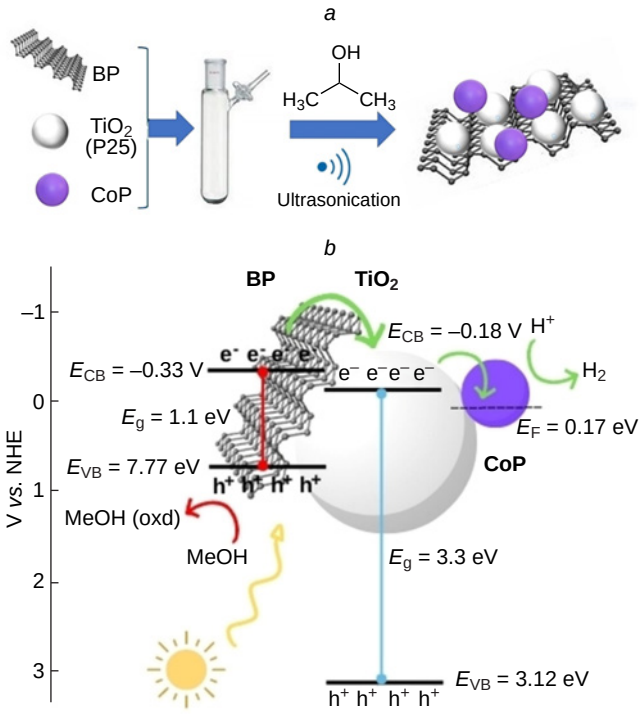

Figure 13. Schematic for the synthesis of the TiO_2/FLBP/CoP ternary heterostructure (*a*) and band energy level diagram and the photocatalytic reaction pathway on the TiO_2/BP/CoP composite under UV-Vis irradiation (*b*).[183] E_F is the Fermi level. Published under a CC BY license from Wiley.

Electrocatalytic systems for hydrogen evolution are also currently being developed. For example, PtRu NPs supported on a microcrystalline cellulose film, with a current density of 88 mA cm^{-2} at a potential of –70 mV *vs* a reversible hydrogen electrode (RHE), are an order of magnitude superior to a commercial Pt/C catalyst.[112] Furthermore, this catalyst exhibited an exceptionally low Tafel slope (19 mV dec^{-1}), indicating fast charge transfer kinetics, as well as high catalyst efficiency and activity. Using DFT calculations, the authors found that the catalyst's high activity is due to strong electronic interactions between PtRu and the FLBP surface. Calculation results showed that the electronic synergistic effects arising from the interaction of the FLBP and ruthenium atoms provide accelerated water dissociation kinetics and optimal hydrogen atom adsorption energy. This, in turn, significantly increases the catalytic activity of platinum atoms in the hydrogen evolution reaction.

Systems free of expensive platinum elements are also of interest. Among such systems, a heterostructure of Ni_2P NPs supported on a FLBP surface exhibited key electrochemical characteristics similar to those of the most common Pt-based electrocatalytic hydrogen production systems.[133,134] Among non-metallic systems, an NH_2-functionalized FLBP demonstrated high activity in the hydrogen evolution reaction: it had an overpotential of 290 mV at a current density of –10 mA cm^{-2}.[104]

As mentioned above, FLBP-based materials can be used as catalysts for oxygen evolution and oxygen reduction reactions.[113,114,119,132,138,139,144,169] Theoretical calculations showed that the pristine FLBP is inactive in these processes due to the high adsorption of O* intermediates on the material surface. However, partial oxidation of FLBP impairs O*

Table 2. Photocatalytic systems for hydrogen evolution based on few-layer black phosphorus.

Catalyst	Light source	Donor of electrons	Activity, μmol h^{-1} g^{-1}	Ref.
FLBP	Xe 300 W, $\lambda > 420$ nm	Na_2S/Na_2SO_3	28	103
FLBP	$\lambda > 420$ nm	Triethanolamine	55	179
FLBP $InCl_3$	$\lambda > 420$ nm	Triethanolamine	2060	159
FLBP/$B(C_6F_5)_3$	$\lambda > 420$ nm	Triethanolamine	6600	159
FLBP–OH	Xe 300 W, $\lambda > 420$ nm	Na_2S/Na_2SO_3	512	103
FLBP/g-C_3N_4	$\lambda > 420$ nm	Triethanolamine	384	179
FLBP/g-C_3N_4	Xe 320 W, $\lambda > 420$ nm	Methanol	427	182
FLBP/$BiVO_4$	$\lambda > 420$ nm	–	160	181
FLBP/MoS_2	Halogen 100 W	Triethanolamine	26800	180
FLBP/$MoSe_2$	Halogen 100 W	Triethanolamine	20700	180
TiO_2/FLBP	Xe 300 W, $\lambda > 420$ nm	Methanol	830	183
TiO_2/FLBP/CoP	Xe 300 W, $\lambda > 420$ nm	Methanol	7400	183

adsorption and increases the material's activity in oxygen evolution and reduction reactions.[184]

Shaijumon and co-workers[73] demonstrated that nitrogen-doped BP quantum dots significantly outperformed the pristine material in the electrochemical production of oxygen from water. Furthermore, Yang's group[138] synthesized two-dimensional transition metal phosphides *via* solvothermal method and successfully applied them in oxygen production reactions. Thus, the two-dimensional $Co_{1.5}Fe_{0.5}P$ phosphide showed an overpotential of 278 mV at a current density of 10 mA cm^{-2} (η_{10}) during oxygen evolution (Fig. 14), which exceeds the similar parameter of reference catalytic systems based on Ir and Ru. The NiN_3/Ni_2P/FLBP nanocomposite demonstrated even higher activity in this process: its overpotential value η_{10} was 247 mV.[185]

In recent years, catalytic water splitting systems have been developed in which the cathodic and anodic reactions are catalyzed by FLBP-based materials. Wang *et al.*[136] modified FLBP with Co_2P cobalt phosphides and used this material as a catalyst for overall water electrolysis. The FLBP/Co_2P nanocomposite showed high catalytic activity in hydrogen and oxygen evolution reactions in an alkaline medium with overpotential values of 336 and 517 mV, respectively, at a current density of 100 mA cm^{-2}. At the same time, the FLBP/Co_2P||FLBP/Co_2P overall water splitting catalytic system required a voltage of 1.92 V to achieve a current density of 10 mA cm^{-2}.

Zhai *et al.*[170] obtained highly active hydrogen and oxygen evolution catalysts based on FLBP modified with Ni_3Pd_1 and Ni_3Fe_1 nanoclusters. The FLBP/Ni_3Pd_1 nanocomposite showed excellent activity in the electrochemical hydrogen evolution

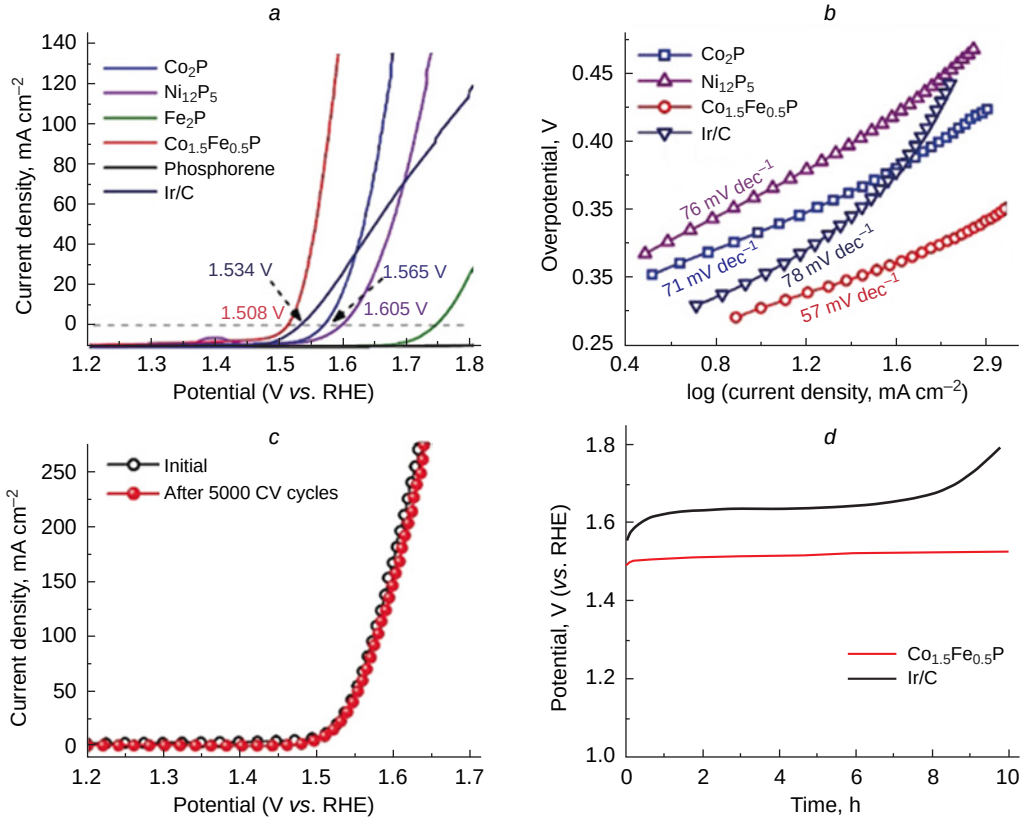

Figure 14. Electrochemical properties of 2D transition metal phosphides in oxygen evolution reaction: oxygen evolution reaction polarization curves of various electrocatalysts (*a*) and the corresponding Tafel plots (*b*); polarization curves of 2D $Co_{1.5}Fe_{0.5}P$ before and after 5000 CV cycles (*c*); results of the long-term stability test of $Co_{1.5}Fe_{0.5}P$ and Ir/C at a current density of 10 mA cm^{-2} (*d*). [138] Published under a CC BY license from Wiley.

reaction with a low overpotential of 53 mV at a current density of 10 mA cm^{-2}. At the same time, the FLBP/Ni_3Fe_1 nanocomposite performed well in the oxygen evolution process with $\eta_{10} = 268$ mV. Furthermore, the FLBP/Ni_3Pd_1||FLBP/Ni_3Fe_1 total water electrolysis system required a very low cell voltage of 1.60 V to achieve a current density of 10 mA cm^{-2} and demonstrated long-term stability, indicating its potential for use in this process.

Liang *et al*.[186] developed an approach to modifying FLBP with cobalt and nickel sulfoselenides. The NiCoSeS/FLBP material demonstrated overpotential values of 172 and 285 mV, respectively, during the electrochemical hydrogen and oxygen evolution. At the same time, a NiCoSeS/FLBP||NiCoSeS/FLBP overall water electrolysis system required a voltage of 1.67 V to achieve a current of 10 mA cm^{-2}.

Table 3 presents comparative characteristics of catalytic FLBP-based systems for the processes of electrochemical hydrogen and oxygen evolution.

Successful examples of developing photocatalytic water-splitting FLBP-based systems have been reported. For example, Majima and co-workers[181] synthesized a heterostructure based on FLBP/$BiVO_4$ and studied its photocatalytic water splitting performance under visible light irradiation. Efficient charge separation *via* the Z-scheme, combined with the low reduction potential of FLBP and the high oxidation potential of $BiVO_4$, led to high activity of the system in pure water in the absence of additional electron donors. The resulting hydrogen (160 μmol g^{-1} h^{-1}) and oxygen (102 μmol g^{-1} h^{-1}) evolution rates indicate great potential for the application of this system in photocatalytic water splitting.

Table 3. Few-layer black phosphorus-based electrocatalysts for hydrogen and oxygen evolution reactions.

Catalyst	Overvoltage (*vs* RHE) at 10 mA cm^{-2}, mW	Tafel slop, mV dec^{-1}	Ref.
Hydrogen evolution reaction			
FLBP	840	293	142
FLBP/PtRu	22	19	112
FLBP/Ni_2P	107	39	133
FLBP/Ni_2P	185	81	134
FLBP–NH_2	290	63	104
FLBP/PdCu	107	103	132
FLBP/Ru	620	180	142
FLBP/Rh	120	79	142
FLBP/Pd	110	212	142
FLBP/Co_2P	336[a]	72	136
FLBP/Co_1	294	107	169
FLBP/Ni_3Pd_1	53	50	170
NiCoSeS/FLBP	172	128	186
Oxygen evolution reaction			
FLBP	380	114	119
FLBP/Co	310	61	114
FLBP/Au	160	68	119
$Co_{1.5}Fe_{0.5}P$	278	57	138
FLBP/CoP	300	56	139
FLBP Ni-Co	292	53	144
NiN_3/Ni_2P/FLBP	247	79	185
FLBP/Co_2P	517[a]	78	136
FLBP/Ni_3Fe_1	268	69	170
NiCoSeS/FLBP	285	116	186

[a] At 100 mA cm^{-2}.

6.2. Carbon dioxide reduction

Electro- and photocatalytic CO_2 reduction is a sustainable green chemistry strategy aimed at reducing the carbon footprint by converting CO_2 into valuable products such as carbon(II) monoxide, methanol, formic acid, methane, and C_2 and C_{2+} hydrocarbons.[187,188] Currently, there are many examples of photo- and electrocatalytic CO_2 reduction systems based on 2D materials, such as atomic layers of transition metals, their oxides, molybdenum and tungsten dichalcogenides, graphene-based materials, and others.[189,190] These materials have high surface energy, a large number of active centres, high electrical conductivity and are actively used to modify electrodes in various processes.

To date, there are studies in which FLBP nanocomposites serve as catalysts. For example, photocatalytic systems for the reduction of CO_2 to CO have been created using hydroxyl-modified FLBP, as well as heterostructures with other semiconductor materials, such as FLBP/g-C_3N_4 (Table 4).[191,192] The $CsPbBr_3$/FLBP system demonstrated high activity in reduction of CO_2 to CO, with an activity of 145 μmol h^{-1} g_{cat}^{-1}.[193] The use of a catalyst based on FLBP quantum dots anchored on WO_3 nanowires in the photocatalytic reduction of CO_2 also yields a significant amount of ethylene in addition to CO.[194]

Heterostructures based on FLBP modified with metal-containing moieties are promising materials for photocatalytic CO_2 conversion.[168,195,196] For example, Ren *et al*.[168] developed a photocatalyst for CO_2 reduction to CO based on FLBP modified with single Co atoms. The process was carried out in the presence of triethanolamine, which acts as an electron donor, and the $[Ru(bipy)_3]Cl_2$ complex used as a photosensitizer. The activity of the resulting catalyst in the photocatalytic reduction of CO_2 was ~89 μmol h^{-1} g^{-1}. Important results were also achieved by modifying FLBP with transition metal phosphides.[196–198] Thus, Co_2P/FLBP heterostructures demonstrated high activity in the reduction of CO_2 to CO (255 μmol h^{-1} g^{-1}).[197] At the same time, the use of the ternary Co_2P@FLBP/g-C_3N_4 system improved the selectivity of this process to 96%.[198]

Table 4. FLBP-based photocatalytic systems for CO_2 reduction.

Catalyst	Light source	Reduction product	Activity, μmol h^{-1} g^{-1}	Ref.
FLBP	Xe 300 W, $\lambda > 420$ nm	CO	25	191
FLBP	Xe 300 W	CO	97	192
FLBP–OH	Xe 300 W, $\lambda > 420$ nm	CO	113	191
FLBP/g-C_3N_4	Xe 300 W	CO	188	192
$CsPbBr_3$/FLBP	Xe 200 W	CO CH_4	134 32	193
WO_3/FLBP	$\lambda > 420$ nm	CO C_2H_4	34 6	194
FLBP/Co	Xe 300 W, $\lambda > 420$ nm	CO	89	168
Co_2P/FLBP	Xe 300 W, $\lambda > 420$ nm	CO	255	197
Co_2P/FLBP/g-C_3N_4	Xe 300 W	CO	16	198

Unlike photocatalytic systems, the development of FLBP-based CO_2 reduction electrocatalysts has faced a number of challenges: surface modification of the material often leads to increased catalytic activity in the hydrogen evolution reaction, complicating fine-tuning the active sites for selective CO_2 reduction. Therefore, to date, only a few examples of the successful use of FLBP-based materials in the electrocatalytic conversion of CO_2 have been reported.[143,199]

Huang *et al.*[199] electrodeposited bismuth dendrites on BP nanosheets and showed this material to be an active catalyst for the reduction of CO_2 to formic acid. The maximum current efficiency of formic acid was 92% at an overpotential of –1.0 V, and the rate of product formation in this process reached 440 μmol dm^{-3} h^{-1}. The Pd-i-BP material also demonstrated high selectivity for formic acid formation during the electrocatalytic reduction of CO_2 (Fig. 15).[143] In addition, the authors note the high stability of the catalyst: the Faradaic efficiency of formic acid production did not fall below 90% for more than 50 h while maintaining a high current density (17 mA cm^{-2} at a potential of –1.0 V).

6.3. Nitrogen reduction

Ammonia is an essential chemical compound widely used in industry and agriculture. It is a key reagent for the synthesis of fertilizers, dyes, polymers, explosives and other important chemical products. Annual ammonia production exceeds 200 million tons, 80% of which is used to produce nitrogen fertilizers. Currently, over 90% of all ammonia is produced *via* the Haber-Bosch process, which is carried out at high temperatures (350–550°C) and pressures (150–350 atm) using an iron-based catalyst.[200] Hydrogen H_2, which is necessary for nitrogen reduction in this process, is produced through high-temperature reactions involving H_2O and various carbon-containing compounds (methane and its homologues, coke, CO, MeOH, *etc.*). The ammonia production process annually accounts for ~3–5% of global methane consumption, 1–2% of energy production, and up to 1.6% of CO_2 emissions.[200,201] Therefore, the development of new catalytic systems capable of producing ammonia under mild conditions and with minimal emissions of harmful substances into the environment is a critical task in modern chemistry.

Due to the similarity of the electronic structures of phosphorus and nitrogen, high surface energy, and the presence of lone electron pairs on the phosphorus atoms, FLBP is a promising material for photo- and electrocatalytic activation of N_2.[202] The ultra-thin two-dimensional structure of phosphorene provides high surface energy and a high concentration of active sites for catalysis. This, in turn, provides higher N_2 adsorption on its surface and increases the efficiency of catalytic reduction. Furthermore, the band gap, tunable depending on the number of layers, facilitates the absorption of a broad spectrum of wavelengths, which is essential for photochemical processes.

Since photochemical and electrochemical reduction of nitrogen to ammonia is typically carried out in an aqueous media, one of the main side reactions is hydrogen evolution. A key advantage of FLBP is the low adsorption of hydrogen on its surface, which hampers hydrogen evolution. The low catalytic activity of FLBP in this competing process allows for the creation of highly selective catalytic systems for the nitrogen reduction reaction.

First tests of FLBP in the catalytic synthesis of ammonia yielded very promising results. In 2018, the Ding's research group[202] first used FLBP as a catalyst for the electrochemical reduction of nitrogen. The process was carried out in an H-type cell in a nitrogen-saturated 0.01 M HCl solution. The highest ammonia production activity was observed at a potential of –0.7 V (*vs* RHE) and amounted to ~31 μg h^{-1} mg_{cat}^{-1}. However, it is worth noting that the maximum Faradaic efficiency of this process was low (~5%), so FLBP-based electrocatalysts needed for additional research aimed at optimizing key catalytic parameters.

Excellent results were also achieved using FLBP in photocatalytic ammonia production. Yu and co-workers[203] developed an approach to producing FLBP with a developed surface area through chemical etching of the material. This catalyst demonstrated exceptionally high ammonia production (2.37 mmol h^{-1} g_{cat}^{-1}) under visible light irradiation comparable to the performance of the most efficient photocatalytic nitrogen fixation systems.

In addition, photoelectrocatalytic nitrogen reduction systems have now been developed. For example, Liu and co-workers[204] modified an indium tin oxide (ITO) electrode with FLBP particles and used it for the photoelectrochemical production of ammonia. This catalyst demonstrated high activity in this process in a nitrogen-saturated electrolyte without the use of additional sacrificial agents. The ammonia formation rate was ~102 μg h^{-1} g_{cat}^{-1}, and the Faradaic efficiency reached ~23% at a potential of –0.4 V (*vs* RHE), exceeding the performance of many known non-metallic catalysts for this reaction. The authors

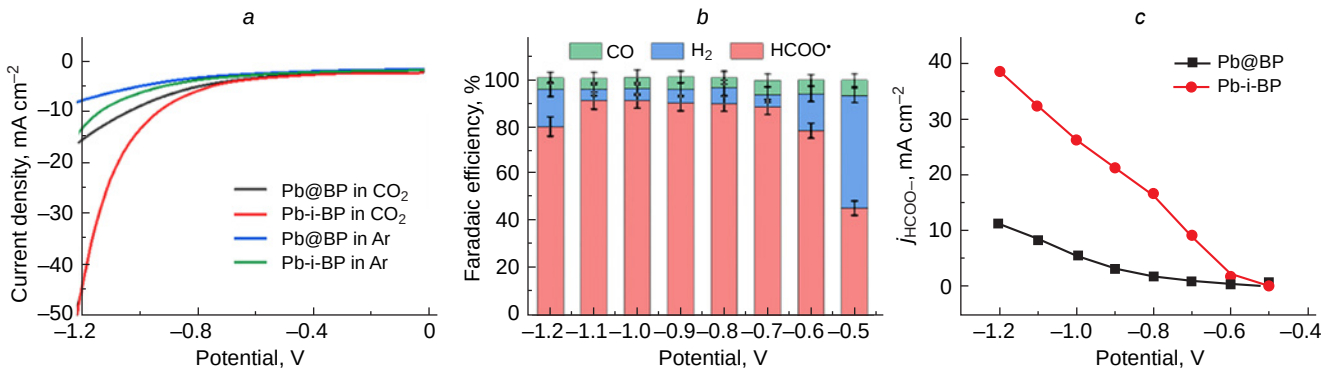

Figure 15. Linear-sweep voltammetry curves for Pd-i-BP and Pd@BP nanosheets in CO_2-saturated or argon-saturated 0.1 M $KHCO_3$ solution (*a*); Faradaic efficiencies for $HCOO^-$, CO and H_2 formation in the electrocatalytic CO_2 reduction (*b*) long-term stability test for the Pd-i-BP catalyst in CO_2 reduction at a potential of –1.0 V *vs* RHE) (*c*).[143] Published under a CC BY-NC 4.0 license from AAAS.

note the synergistic effect of conducting the reaction in photoelectrochemical mode: electrolysis under light irradiation provided significantly higher ammonia formation efficiency than in the case of separate electrocatalytic and photocatalytic nitrogen reduction. Photoexcitation of electrons from the valence band to the conduction band was found to significantly improve the material's electrical conductivity, enhancing its activity in electrochemical processes. In turn, the applied cathodic potential accelerates the recovery of photogenerated holes, further enhancing the photocatalytic efficiency of FLBP.

To improve the stability of FLBP under environmental conditions, various heterostructures based thereon are created. Thus, to date, FLBP structures with CdS NPs,[205] FLBP quantum dots anchored on SnO_{2-x} nanotubes[206] and MnO_2 nanosheets,[207] as well as 2D/2D FLBP/g-C_3N_4 heterostructures have been obtained.[208] These materials have demonstrated high catalytic activity in photochemical nitrogen fixation processes.

The research group of Professor Ding[209] developed catalysts based on FLBP functionalized with Al^{3+} ions, which demonstrated high activity in ammonia production (~55 μg h^{-1} mg^{-1}) with a Faradaic efficiency of ~66%. This work also demonstrated that functionalization of black phosphorus with Al^{3+} ions improves catalyst stability under electrochemical experimental conditions due to the formation of Al–P bonds *via* a donor-acceptor mechanism, thereby protecting the material surface from environmental influences. The same research group[210] also proposed a strategy for producing environmentally stable FLBP by simultaneously creating defects and fluoride protection based on topochemical reactions of BP. Fluorine-stabilized FLBP demonstrated high activity (~70 μg h^{-1} mg_{cat}^{-1}) and Faradaic efficiency (~26%) at a potential of –0.5 V (*vs* RHE) in the electrocatalytic reduction of nitrogen to NH_3 in an aqueous electrolyte.

Doping the surface of FLBP with certain elements also improves the catalytic activity of the material. According to DFT calculations, FLBP sheets doped with molybdenum and boron exhibit high performance in nitrogen fixation processes.[211] Ma and co-workers[212] described the production of N-doped FLBP using a combination of ball milling and microwave irradiation. It was found that thus modified material shows high electrocatalytic performance in the ammonia synthesis: the catalyst productivity was ~19 μg h^{-1} mg^{-1} with a Faradaic efficiency of ~22%. Wang and co-workers[213] developed a mechanochemical approach to obtain the Fe_4P/FLBP heterostructure by milling a mixture of red phosphorus and iron microparticles in a ball mill. The resulting material catalyzes the reduction of nitrogen to ammonia at a potential of –0.2 V, demonstrating a selectivity of ~63% and an activity of ~78 μg h^{-1} mg^{-1}. These parameters are comparable to those of the most effective catalytic systems for this process. Furthermore, DFT calculations shed light on the catalytic mechanism. It has been shown that phosphorus atoms in FLBP and Fe_4P are involved in proton adsorption, forming P–H moieties, which in turn facilitate the activation of the N_2 molecule to form the NNH* intermediate. Iron atoms in Fe_4P phosphide interact with this intermediate to promote its further reduction.

7. Conclusion

Due to its unique physical properties, FLBP occupies a worthy place among two-dimensional materials. Despite significant advances in research on this material in recent years, several fundamental challenges remain for the scientific community to solve before FLBP can be fully implemented in practice. One important task is the development of new approaches to the synthesis of BP.[47] The existing laboratory method for synthesizing BP, based on the gas-transport transformation of red phosphorus, while meeting the needs of fundamental research, does not satisfy the requirements of industrial production. Therefore, the development of new approaches for the large-scale synthesis of high-quality BP requires additional efforts.

Furthermore, considerable attention is being paid to improving methods for producing FLBP.[8,31] To date, a large number of methods for preparing FLBP based on the exfoliation of BP have been developed. Among these, the most widely used is the sonication-assisted liquid-phase exfoliation of BP. However, approaches that produce exfoliated material of high quality and in higher yields in a shorter time are of great interest. From this perspective, the most promising approach is considered to be electrochemical exfoliation of BP, which is increasingly being used to produce FLBP in research studies.[76]

One of the most pressing problems is the low stability of FLBP under environmental conditions.[18,21] Therefore, significant research efforts are focused on chemical surface modification and material functionalization to prevent oxidation and degradation processes. Various strategies for covalent and non-covalent functionalization of FLBP have been proposed, as well as approaches to creating hybrid structures with transition metal nanoparticles.[22,24,89] Despite a number of significant achievements, this area still requires further research, including the use of new reagents and the development of new methods for modifying the FLBP surface. Furthermore, a key challenge remains a poor understanding of the mechanisms of interaction between FLBP and modifying substrates. In this context, the use of computer modelling methods, particularly DFT calculations, can become a powerful tool for predicting and explaining the observed effects.

Decorating FLBP with transition metal nanoparticles not only increases the material's stability but also imparts unique catalytic properties.[24] Due to synergistic effects in 0D/2D hybrid systems, such materials demonstrate outstanding results in small molecule activation processes. In particular, they have been used to create electro- and photocatalytic systems for reactions of hydrogen and oxygen evolution, carbon dioxide reduction and molecular nitrogen fixation.[25,27,28,171,214] However, despite the existing successful examples, more systematic studies aimed at elucidating clear correlations between the structure of catalysts and their functional characteristics are needed to fully realize the potential of FLBP in catalysis.

In the context of developing efficient, highly selective, and atom-efficient catalytic systems, the creation of single-atom catalysts has seen widespread development in the last decade. From this perspective, FLBP, representing a giant two-dimensional polyphosphorus ligand, is considered an ideal support for metal active sites. To date, only the first successful steps have been taken towards creating FLBP-based single-atom catalysts, offering great opportunities for future research. A key challenge is developing methods for the controlled engineering of defects on the FLBP surface, as defect sites serve as the most effective anchoring centres for stabilizing metal atoms. The potential of this approach is underscored by its analogy with classical homogeneous catalysis, where phosphine ligands have long been successfully used to stabilize metal complexes. Consequently, FLBP-based single-atom catalysts have the potential to become heterogeneous embodiments of such highly effective catalytic systems, combining the selectivity inherent in molecular complexes with the practical advantages of

heterogeneous catalysts, *viz*., stability and ease of separation from the reaction mixture. This makes this approach one of the most promising in the design of new catalytic materials.

In conclusion, it should be emphasized that black phosphorus-based materials continue to be the focus of intensive research due to their unique combination of properties. Further development of black phosphorus chemistry could lead to breakthroughs in green energy, eco-catalysis and the development of new functional materials. Successfully addressing the challenges facing researchers will not only expand fundamental knowledge of two-dimensional materials but also create technological solutions that facilitate the transition to sustainable development and reduce anthropogenic impact on the environment. Thus, research in the field of black phosphorus chemistry represents a striking example of how fundamental scientific research can lead to practical results that are crucial for solving global problems.

This review was financially supported by the Russian Science Foundation (Project No. 23-13-00427).

8. List of abbreviations and designations

η_{10} — overpotential at current density of 10 mA cm^{-2};
AFM — atomic force microscopy;
BP — black phosphorus;
bipy — 2,2′-bipyridine;
Cp — cyclopentadienyl;
DFT — density functional theory;
EMIM — 1-ethyl-3-methylimidazolium;
EXAFS — extended X-ray absorption fine structure;
FLBP — few-layer black phosphorus;
g-C_3N_4 — graphitic carbon nitride;
HAADF-STEM — high-angle annular dark-field scanning transmission electron microscopy;
hfac — hexafluoroacetylacetonate;
HSAB — hard and soft acids and bases;
ITO — indium-tin oxide;
NMP — *N*-methylpyrrolidone;
NP — nanoparticles;
RHE — reversible hydrogen electrode;
RT — room temperature;
SHE — standard hydrogen electrode;
TEM — transmission electron microscopy;
TMNP — transition metal nanoparticles;
XANES — X-ray absorption near-edge structure;
XPS — X-ray photoelectron microscopy;
XRPD — X-ray powder diffraction.

9. References

1. K.S.Novoselov, A.Mishchenko, A.Carvalho, A.H.Castro Neto. *Science*, **353** (6298), aac9439 (2016); https://doi.org/10.1126/science.aac9439
2. R.Mas-Ballesté, C.Gómez-Navarro, J.Gómez-Herrero, F.Zamora. *Nanoscale*, **3**, 20 (2011); https://doi.org/10.1039/c0nr00323a
3. K.S.Novoselov, A.K.Geim, S.V.Morozov, D.Jiang, Y.Zhang, S.V.Dubonos. *Science*, **306** (5696), 666 (2004); https://doi.org/10.1126/science.1102896
4. S.Balendhran, S.Walia, H.Nili, S.Sriram, M.Bhaskaran. *Small*, **11** (6), 640 (2015); https://doi.org/10.1002/smll.201402041
5. X.Ren, P.Lian, D.Xie, Y.Yang, Y.Mei, X.Huang, Z.Wang, X.Yin. *J. Mater Sci*., **52** (17), 10364 (2017); https://doi.org/10.1007/s10853-017-1194-3
6. R.Gusmão, Z.Sofer, M.Pumera. *Angew. Chem., Int. Ed*., **56** (28), 8052 (2017); https://doi.org/10.1002/anie.201610512
7. S.Bagheri, N.Mansouri, E.Aghaie. *Int. J. Hydrogen Energy*, **41** (7), 4085 (2016); https://doi.org/10.1016/j.ijhydene.2016.01.034
8. A.H.Woomer, T.W.Farnsworth, J.Hu, R.A.Wells, C.L.Donley, S.C.Warren. *ACS Nano*, **9** (9), 8869 (2015); https://doi.org/10.1021/acsnano.5b02599
9. S.P.Koenig, R.A.Doganov, H.Schmidt, A.H.Castro Neto, B.Özyilmaz. *Appl. Phys. Lett*., **104** (10), 103106 (2014); https://doi.org/10.1063/1.4868132
10. A.Castellanos-Gomez, L.Vicarelli, E.Prada, J.O'Island, K.L.Narasimha-Acharya, S.I.Blanter, D.J.Groenendijk, M.Buscema, G.A.Steele, J.V.Alvarez, H.W.Zandbergen, J.J.Palacios, H.S.J.van der Zant. *2D Mate*rials, **1** (2), 025001 (2014); https://doi.org/10.1088/2053-1583/1/2/025001
11. J.D.Wood, S.A.Wells, D.Jariwala. K.-S.Chen, E.K.Cho, V.K.Sangwan, X.Liu, L.J.Lauhon. T.J.Marks, M.C.Hersam. *Nano Lett*., **14** (12), 6964 (2014); https://doi.org/10.1021/nl5032293
12. H.Liu, A.T.Neal, Z.Zhu, Z.Luo, X.Xu, D.Tománek, P.D.Ye. *ACS Nano*, **8** (4), 4033 (2014); https://doi.org/10.1021/nn501226z
13. S.C.Dhanabalan, J.S.Ponraj, Z.Guo, S.Li, Q.Bao, H.Zhang. *Adv. Sci*., **4** (6), 1600305 (2017); https://doi.org/10.1002/advs.201600305
14. Y.Yang, M.Wu, X.Zhu, H.Xu, S.Ma, Y.Zhi, H.Xia, X.Liu, J.Pan, J.-Y.Tang, S.-P.Chai, L.Palmisano, F.Parrino, J.Liu, J.Ma, Z.-L.Wang, L.Tan, Y.-F.Zhao, Y.-F.Song, P.Singh, P.Raizada, D.Jiang, D.Li, R.A.Geioushy, J.Ma, J.Zhang, S.Hu, R.Feng, G.Liu, M.Liu, Z.Li, M.Shao, N.Li, J.Peng, W.-J.Ong, N.Kornienko, Z.Xing, X.Fan, J.Ma. *Chin. Chem. Lett*., **30** (12), 2065 (2019); https://doi.org/10.1016/j.cclet.2019.11.001
15. A.Jain, A.J.H.McGaughey. *Sci. Rep*., **5**, 8501 (2015); https://doi.org/10.1038/srep08501
16. S.Walia, Y.Sabri, T.Ahmed, M.R.Field, R.Ramanathan, A.Arash, S.K.Bhargava, S.Sriram, M.Bhaskaran, V.Bansal, S.Balendhranl. *2D Materials*, **4** (1), 015025 (2017); https://doi.org/10.1088/2053-1583/4/1/015025
17. Q.Zhou, Q.Chen, Y.Tong, J.Wang. *Angew. Chem., Int. Ed*., **55** (38), 11437 (2016); https://doi.org/10.1002/anie.201605168
18. J.O.Island, G.A.Steele, H.S.J.Van Der Zant, A.Castellanos-Gomez. *2D Materils*, **2** (1), 11002 (2015); https://doi.org/10.1088/2053-1583/2/1/011002
19. M.Van Druenen, F.Davitt, T.Collins, C.Glynn, C.O'Dwyer, J.D.Holmes, G.Collins. *Chem. Mater*., **30** (14), 4667 (2018); https://doi.org/10.1021/acs.chemmater.8b01306
20. S.Kuriakose, T.Ahmed, S.Balendhran, S.Sriram, M.Bhaskaran, S.Walia. *2D Materials*, **5** (3), 032001 (2018); https://doi.org/10.1088/2053-1583/aab810
21. A.Favron, E.Gaufrès, F.Fossard, A.-L.Phaneuf-L'Heureux, N.Y-W.Tang, P.L.Lévesque, A.Loiseau, R.Leonelli, S.Francoeur, R.Martel. *Nat. Mater*., **14** (8), 826 (2015); https://doi.org/10.1038/nmat4299
22. Y.Liu, M.Chen, S.Yang. *InfoMat*., **3** (3), 231 (2021); https://doi.org/10.1002/inf2.12171
23. M.Peruzzini, R.Bini, M.Bolognesi, M.Caporali, M.Ceppatelli, F.Cicogna, S.Coiai, S.Heun, A.Ienco, I.I.Benito, A.Kumar, G.Manca, E.Passaglia, D.Scelta, M.Serrano-Ruiz, F.Telesio, S.Toffanin, M.Vanni. *Eur. J. Inorg. Chem*., (11–12), 1476 (2019); https://doi.org/10.1002/ejic.201801219
24. Aid.M.Kuchkaev, S.Lavate, Air.M.Kuchkaev, A.V.Sukhov, R.Srivastava, D.G.Yakhvarov. *Energy Technol*., **9** (12), 2100581 (2021); https://doi.org/10.1002/ente.202100581
25. X.Li, J.Wang. *Adv. Mater. Interfaces*, **7** (18), 2000676 (2020); https://doi.org/10.1002/admi.202000676
26. F.Shi, K.Huang, S.Feng. *ChemCatChem*., **12** (7), 1913 (2020); https://doi.org/10.1002/cctc.201902288
27. T.H.Lee, S.Y.Kim, H.W.Jang. *Nanomaterials*, **6** (11), 194 (2016); https://doi.org/10.3390/nano6110194

28. W.Gao, Y.Zhou, X.Wu, Q.Shen, J.Ye, Z.Zou. *Adv. Funct. Mater*., **31** (3), 2005197 (2021); https://doi.org/10.1002/adfm.202005197
29. R.K.Mishra, J.Sarkar, I.Chianella, S.Goel, H.Y.Nezhad. *Next Mater.*, **4**, 100217 (2024); https://doi.org/10.1016/j.nxmate.2024.100217
30. F.Xia, H.Wang, Y.Jia. *Nat. Commun*., **5**, 4458 (2014); https://doi.org/10.1038/ncomms5458
31. D.Roy, P.Pal, T.Pal, R.A.Doong. *Appl. Mater. Today*, **35**, 101944 (2023); https://doi.org/10.1016/j.apmt.2023.101944
32. J.W.Jiang, H.S.Park. *J. Phys. D: Appl. Phys*., **47** (38), 385304 (2014); https://doi.org/10.1088/0022-3727/47/38/385304
33. J.Tao, W.Shen, S.Wu, L.Liu, Z.Feng, C.Wang, C.Hu, P.Yao, H.Zhang, W.Pang, X.Duan, J.Liu, C.Zhou, D.Zhang. *ACS Nano*, **9** (11), 11362 (2015); https://doi.org/10.1021/acsnano.5b05151
34. L.Li, W.Han, L.Pi, P.Niu, J.Han, C.Wang, B.Su, H.Li, J.Xiong, Y.Bando, T.Zhai. *InfoMat*, **1** (1), 54 (2019); https://doi.org/10.1002/inf2.12005
35. W.Zhou, T.Pan, H.Cui, Z.Zhao, P.K.Chu, X.F.Yu. *Angew. Chem., Int. Ed*., **58** (3), 769 (2019); https://doi.org/10.1002/anie.201810878
36. S.Geng, T.Pan, W.Zhou, H.Cui, L.Wu, Z.Li, P.K.Chu, X.F.Yu. *Theranostics*, **10** (11), 4720 (2020); https://doi.org/10.7150/thno.43092
37. W.Tao, X.Zhu, X.Yu, X.Zeng, Q.Xiao, X.Zhang, X.Ji, X.Wang, J.Shi, H.Zhang, L.Mei. *Adv. Mater*., **29** (1), 1603276 (2017); https://doi.org/10.1002/adma.201603276
38. W.Fu, W.Zhou, P.K.Chu, X.F.Yu. *Chem. – Eur. J.*, **25** (47), 10995 (2019); https://doi.org/10.1002/chem.201901841
39. J.Ding, G.Qu, P.K.Chu, X.F.Yu. *VIEW*, **2** (1), 20200043 (2021); https://doi.org/10.1002/VIW.20200043
40. A.Bigham, M.Serrano-Ruiz, M.Caporali, I.Fasolino, M.Peruzzini, L.Ambrosio, M.G.Raucci. *Chem. Soc. Rev*., **54**, 827 (2025); https://doi.org/10.1039/d4cs00007b
41. P.W.Bridgman. *J. Am. Chem. Soc*., **36** (7), 1344 (1914); https://doi.org/10.1021/ja02184a002
42. E.I.Jahre, D.Phosphor, W.Gunther, D.P.Stofidrucken, H.Krebs, H.Weitz, K.Worms. *J. Inorg. Chem*., **280** (1–3), 119 (1943)
43. A.Brown, S.Rundqvist. *Acta Crystallogr*., **19** (4), 684 (1965); https://doi.org/10.1107/s0365110x65004140
44. T.Nilges, M.Kersting, T.Pfeifer. *J. Solid State Chem*., **181** (8), 1707 (2008); https://doi.org/10.1016/j.jssc.2008.03.008
45. M.Köpf, N.Eckstein, D.Pfister, C.Grotz, I.Krüger, M.Greiwe, T.Hansen, H.Kohlmann, T.Nilges. *J. Cryst. Growth*, **405**, 6 (2014); https://doi.org/10.1016/j.jcrysgro.2014.07.029
46. S.Lange, P.Schmidt, T.Nilges. *Inorg Chem*., **46** (10), 4028 (2007); https://doi.org/10.1021/ic062192q
47. K.N.Dinh, Y.Zhang, W.Sun. *J. Phys. Energy*, **3** (3), 032007 (2021); https://doi.org/10.1088/2515-7655/abf2da
48. Aid.M.Kuchkaev, A.V.Sukhov, Air.M.Kuchkaev, S.A.Ziganshina, V.M.Babaev, A.T.Gubaidullin, A.B.Dobrynin, I.R.Nizameev, R.Shrivastava, S.Lavate, O.G.Sinyashin, D.G.Yakhvarov. *Russ. J. Electrochem*., **58**, 680 (2022); https://doi.org/10.1134/S1023193522080080
49. S.J.Lu, L.Tang, Z.Xiao, M.Zhang, W.Guo, M.Tan, Y.Wan, F.X.Xiao, Y.Lin. *Inorg Chem*., **63** (24), 11092 (2024); https://doi.org/10.1021/acs.inorgchem.4c00655
50. S.Zhang, Z.Qin, Z.Hou, J.Ye, Z.Xu, Y.Qian. *ChemPhysMater*, **1** (1), 1 (2022); https://doi.org/10.1016/j.chphma.2021.09.005
51. S.Hao, X.Zhao, Q.Cheng, Y.Xing, W.Ma, X.Wang, G.Zhao, X.Xu. *Front. Chem*., **8**, 582146 (2020); https://doi.org/10.3389/fchem.2020.582146
52. H.Li, G.Lu, Y.Wang, Z.Yin, C.Cong, Q.He, L.Wang, F.Ding, Ti.Yu, H.Zhang. *Small*, **9** (11), 1974 (2013); https://doi.org/10.1002/smll.201202919
53. M.Yi, Z.Shen. *J. Mater. Chem. A*, **3** (22), 11700 (2015); https://doi.org/10.1039/c5ta00252d
54. K.S.Novoselov, A.H.Caatro Neto. *Phys. Scr*., (T146), 014006 (2012); https://doi.org/10.1088/0031-8949/2012/T146/014006
55. X.Wang, A.M.Jones, K.L.Seyler, V.Tran, Y.Jia, H.Zhao, H.Wang, L.Yang, X.Xu, F.Xia. *Nat. Nanotechnol*., **10** (6), 517 (2015); https://doi.org/10.1038/nnano.2015.71
56. Z.Luo, J.Maassen, Y.Deng, Y.Du, R.P.Garrelts, M.S.Lundstrom, P.D.Ye, X.Xu. *Nat. Commun*., **6** (1), 8572 (2015); https://doi.org/10.1038/ncomms9572
57. R.Xu, S.Zhang, F.Wang, J.Yang, Z.Wang, J.Pei, Y.W.Myint, B.Xing, Z.Yu, L.Fu, Q.Qin, Y.Lu. *ACS Nano*, **10** (2), 2046 (2016); https://doi.org/10.1021/acsnano.5b06193
58. J.Kang, J.D.Wood, S.A.Wells, J.H.Lee, X.Liu, K.S.Chen, M.C.Hersam. *ACS Nano*, **9** (4), 3596 (2015); https://doi.org/10.1021/acsnano.5b01143
59. W.Zhao, Z.Xue, J.Wang, J.Jiang, X.Zhao, T.Mu. *ACS Appl. Mater. Interfaces*, **7** (50), 27608 (2015); https://doi.org/10.1021/acsami.5b10734
60. G.Abellán, S.Wild, V.Lloret, N.Scheuschner, R.Gillen, U.Mundloch, J.Maultzsch, M.Varela, F.Hauke, A.Hirsch. *J. Am. Chem. Soc*., **139** (30), 10432 (2017); https://doi.org/10.1021/jacs.7b04971
61. V.Nicolosi, M.Chhowalla, M.G.Kanatzidis, M.S.Strano, J.N.Coleman. *Science*, **340** (6139), 1226419 (2013); https://doi.org/10.1126/science.1226419
62. K.R.Paton, E.Varrla, C.Backes, R.J.Smith, U.Khan, A.O'Neill, C.Boland, M.Lotya, O.M.Istrate, P.King, T.Higgins, S.Barwich, P.May, P.Puczkarski, I.Ahmed, M.Moebius, H.Pettersson, E.Long, J.Coelho, S.E.O'Brien, E.K.McGuire, B.M.Sanchez, G.S.Duesberg, N.McEvoy, T.J.Pennycook, C.Downing, A.Crossley, V.Nicolosi, J.N.Coleman. *Nat. Mater*., **13** (6), 624 (2014); https://doi.org/10.1038/nmat3944
63. F.Xu, B.Ge, J.Chen, A.Nathan, L.L.Xin, H.Ma, H.Min, C.Zhu, W.Xia, Z.Li, S.Li, K.Yu, L.Wu, Y.Cui, L.Sun, Y.Zhu. *2D Materials*, **3** (2), 025005 (2016); https://doi.org/10.1088/2053-1583/3/2/025005
64. R.Gusmão, Z.Sofer, M.Pumera. *ACS Nano*, **12** (6), 5666 (2018); https://doi.org/10.1021/acsnano.8b01474
65. N.Omura, Y.Hotta, K.Sato, Y.Kinemuchi, S.Kume, K.Watari. *J. Eur. Ceram. Soc*., **27** (2–3), 733 (2007); https://doi.org/10.1016/j.jeurceramsoc.2006.04.001
66. A.E.Del Río Castillo, C.D.Reyes-Vazquez, L.E.Rojas-Martinez, S.B.Thorat, M.Serri, A.L.Martinez-Hernandez, C.Velasco-Santos, V.Pellegrini, F.Bonaccorso. *FlatChem*, **18**, 100131 (2019); https://doi.org/10.1016/j.flatc.2019.100131
67. A.E.Del Rio Castillo, V.Pellegrini, A.Ansaldo, F.Ricciardella, H.Sun, L.Marasco, J.Buha, Z.Dang, L.Gagliani, E.Lago, N.Curreli, S.Gentiluomo, F.Palazon, M.Prato, R.Oropesa-Nuñez, P.S.Toth, E.Mantero, M.Crugliano, A.Gamucci, A.Tomadin, M.Polinia, F.Bonaccorso. *Mater. Horiz*., **5** (5), 890 (2018); https://doi.org/10.1039/c8mh00487k
68. M.Bat-Erdene, M.Batmunkh, C.J.Shearer, S.A.Tawfik, M.J.Ford, L.P.Yu, A.J.Sibley, A.D.Slattery, J.S.Quinton, C.T.Gibson, J.G.Shapter. *Small Methods*, **1** (12), 1700260 (2017); https://doi.org/10.1002/smtd.201700260
69. M.Batmunkh, M.Myekhlai, A.S.R.Bati, S.Sahlos, A.D.Slattery, T.M.Benedetti, V.R.Gonçales, C.T.Gibson, J.J.Gooding, R.D.Tilley, J.G.Shapter. *J. Mater. Chem. A*, **7** (21), 12974 (2019); https://doi.org/10.1039/c9ta02513h
70. A.Ambrosi, Z.Sofer, M.Pumera. *Angew. Chem., Int. Ed*., **56** (35), 10443 (2017); https://doi.org/10.1002/anie.201705071
71. H.Xiao, M.Zhao, J.Zhang, X.Ma, J.Zhang, T.Hu, T.Tang, J.Jia, H.Wu. *Electrochem. Commun*., **89**, 10 (2018); https://doi.org/10.1016/j.elecom.2018.02.010
72. L.Zu, X.Gao, H.Lian, C.Li, Q.Liang, Y.Liang, X.Cui, Y.Liu, X.Wang, X.Cui. *J. Alloys Compd*., **770**, 26 (2019); https://doi.org/10.1016/j.jallcom.2018.07.265
73. R.Prasannachandran, T.V.Vineesh, A.Anil, B.M.Krishna, M.M.Shaijumon. *ACS Nano*, **12** (11), 11511 (2018); https://doi.org/10.1021/acsnano.8b06671
74. J.Li, C.Chen, S.Liu, J.Lu, W.P.Goh, H.Fang, Z.Qiu, B.Tian, Z.Chen, C.Yao, W.Liu, H.Yan, Y.Yu, D.Wang, Y.Wang,

M.Lin, C.Su, J.Lu. *Chem. Mater*., **30** (8), 2742 (2018); https://doi.org/10.1021/acs.chemmater.8b00521
75. Aid.M.Kuchkaev, Air.M.Kuchkaev, A.V.Sukhov, S.V.Saparina, O.I.Gnezdilov, A.E.Klimovitskii, S.A.Ziganshina, I.R.Nizameev, I.P.Asanov, K.A.Brylev, O.G.Sinyashin, D.G.Yakhvarov. *Int. J. Mol. Sci*., **24** (4), 3095 (2023); https://doi.org/10.3390/ijms24043095
76. A.R.Baboukani, I.Khakpour, V.Drozd, C.Wang. *Small Struct*., **2** (5), 2000148 (2021); https://doi.org/10.1002/sstr.202000148
77. M.Wen, D.Liu, Y.Kang, J.Wang, H.Huang, J.Li, P.K.Chu, X.F.Yu. *Mater Horiz*., **6** (1), 176 (2019); https://doi.org/10.1039/c8mh00708j
78. X.Tang, W.Liang, J.Zhao, Z.Li, M.Qiu, T.Fan, C.S.Luo, Y.Zhou, Y.Li, Z.Guo, D.Fan, H.Zhang. *Small*, **13** (47), 1702739 (2017); https://doi.org/10.1002/smll.201702739
79. Y.Fang, X.Li, J.Li, C.Yao, H.Y.Hoh, X.Hai, J.Lu, C.Su. *J. Mater. Chem. A*, **7**, 25691 (2019); https://doi.org/10.1039/c9ta10487a
80. D.Zhou, H.Li, N.Si, H.Li, H.Fuchs, T.Niu. *Adv. Funct. Mater*., **31** (6), 2006997 (2021); https://doi.org/10.1002/adfm.202006997
81. G.Li, Y.Y.Zhang, H.Guo, L.Huang, H.Lu, X.Lin, Y.L.Wang, S.Du, H.J.Gao. *Chem. Soc. Rev*., **47** (16), 6073 (2018); https://doi.org/10.1039/c8cs00286j
82. J.Zhang, F.Wang, V.B.Shenoy, M.Tang, J.Lou. *Mater. Today*, **40**, 132 (2020); https://doi.org/10.1016/j.mattod.2020.06.012
83. Z.Cai, B.Liu, X.Zou, H.M.Cheng. *Chem. Rev*., **118** (13), 6091 (2018); https://doi.org/10.1021/acs.chemrev.7b00536
84. J.Yu, J.Li, W.Zhang, H.Chang. *Chem. Sci*., **6** (12), 6705 (2015); https://doi.org/10.1039/c5sc01941a
85. J.B.Smith, D.Hagaman, H.F.Ji. *Nanotechnology*, **27** (21), 215602 (2016); https://doi.org/10.1088/0957-4484/27/21/215602
86. H.Xu, X.Han, Z.Li, W.Liu, X.Li, J.Wu, Z.Guo, H.Liu. *Adv. Mater. Interfaces*, **5** (21), 1801048 (2018); https://doi.org/10.1002/admi.201801048
87. Bin Tian, Bining Tian, B.Smith, M.C.Scott, Q.Lei, R.Hua, Y.Tian, Y.Liu. *Proc. Natl. Acad. Sci. USA*, **115** (17), 4345 (2018); https://doi.org/10.1073/pnas.1800069115
88. C.M.Park, H.J.Sohn. *Adv. Mater*., **19** (18), 2465 (2007); https://doi.org/10.1002/adma.200602592
89. S.Thurakkal, X.Zhang. *Adv. Sci*., **7** (2), 1902359 (2020); https://doi.org/10.1002/advs.201902359
90. R.Jain, Y.Singh, S.Y.Cho, S.P.Sasikala, S.H.Koo, R.Narayan, H.T.Jung, Y.Jung, S.O.Kim. *Chem. Mater*., **31** (8), 2786 (2019); https://doi.org/10.1021/acs.chemmater.8b04984
91. Y.Zhou, J.Huang, J.Wang, F.Chu, Z.Xu, W.Hu, Y.Hu. *Polym. Degrad. Stabil*., **178**, 109194 (2020); https://doi.org/10.1016/j.polymdegradstab.2020.109194
92. Q.Feng, H.Liu, M.Zhu, J.Shang, D.Liu, X.Cui, D.Shen, L.Kou, D.Mao, J.Zheng, C.Li, J.Zhang, H.Xu, J.Zhao. *ACS Appl. Mater. Interfaces*, **10** (11), 9679 (2018); https://doi.org/10.1021/acsami.8b00556
93. A.Kocaarslan, Z.Eroglu, G.Yilmaz, O.Metin, Y.Yagci. *ACS Macro Lett*., **10** (6), 679 (2021); https://doi.org/10.1021/acsmacrolett.1c00298
94. A.Roucoux, J.Schulz, H.Patin. *Chem Rev*., **102** (10), 3757 (2002); https://doi.org/10.1021/cr010350j
95. C.R.Ryder, J.D.Wood, S.A.Wells, Y.Yang, D.Jariwala, T.J.Marks, G.C.Schatz, M.C.Hersam. *Nat. Chem*., **8** (6), 597 (2016); https://doi.org/10.1038/nchem.2505
96. A.Mitrović, S.Wild, V.Lloret, M.Fickert, M.Assebban, B.G.Márkus, F.Simon, F.Hauke, G.Abellán, A.Hirsch. *Chem. – Eur. J*., **27** (10), 3361 (2021); https://doi.org/10.1002/chem.202003584
97. L.Zhang, L.-F.Gao, L.Li, C.-X.Hu, Q.-Q.Yang, Z.-Y.Zhu, R.Peng, Q.Wang, Y.Peng, J.Jin, H.-L.Zhang. *Mater. Chem. Front*., **2** (9), 1700 (2018); https://doi.org/10.1039/c8qm00237a
98. Aid.M.Kuchkaev, Air.M.Kuchkaev, A.V.Sukhov, S.V.Saparina, O.I.Gnezdilov, A.E.Klimovitskii, S.A.Ziganshina, I.R.Nizameev, B.A.Faizullin, O.G.Sinyashin, D.G.Yakhvarov. *J. Struct. Chem*., **65**, 643 (2024); https://doi.org/10.1134/S0022476624040012
99. S.Wild, M.Fickert, A.Mitrovic, V.Lloret, C.Neiss, J.A.Vidal-Moya, M.Á.Rivero-Crespo, A.Leyva-Pérez, K.Werbach, H.Peterlik, M.Grabau, H.Wittkämper, C.Papp, H.-P.Steinrück, T.Pichler, A.Görling, F.Hauke, G.Abellán, A.Hirsc. *Angew. Chem., Int. Ed.*, **58** (17), 5763 (2019); https://doi.org/10.1002/anie.201811181
100. Aid.M.Kuchkaev, Air.M.Kuchkaev, A.V.Sukhov, S.V.Saparina, O.I.Gnezdilov, A.E.Klimovitskii, S.A.Ziganshina, I.R.Nizameev, I.R.Vakhitov, A.B.Dobrynin, D.I.Stoikov, G.A.Evtugyn, O.G.Sinyashin, X.Kang, D.G.Yakhvarov. *Nanomaterials*, **13** (5), 826 (2023); https://doi.org/10.3390/nano13050826
101. K.L.W.Mitra, C.H.Chang, M.P.Hanrahan, J.Yang, D.Tofan, W.M.Holden, N.Govind, G.T.Seidler, A.J.Rossini, A.Velian. *Angew. Chem., Int. Ed*., **60** (16), 9127 (2021); https://doi.org/10.1002/anie.202016033
102. Y.Liu, P.Gao, T.Zhang, X.Zhu, M.Zhang, M.Chen, P.Du, G.-W.Wang, H.Ji, J.Yang, S.Yang. *Angew. Chem., Int. Ed*., **58** (5), 1479 (2019); https://doi.org/10.1002/anie.201813218
103. X.Zhu, T.Zhang, Z.Sun, H.Chen, J.Guan, X.Chen, H.Ji, P.Du, S.Yang. *Adv. Mater*., **29** (17), 1605776 (2017); https://doi.org/10.1002/adma.201605776
104. L.Shao, H.Sun, L.Miao, X.Chen, M.Han, J.Sun, S.Liu, L.Li, F.Cheng, J.Chen. *J. Mater. Chem. A*, **6** (6), 2494 (2018); https://doi.org/10.1039/c7ta10884b
105. I.Matsui. *J. Chem. Eng. Jpn*., **38** (8), 535 (2005); https://doi.org/10.1252/jcej.38.535
106. Y.Lan, Y.Lu, Z.Ren. *Nano Energy*, **2** (5), 1031 (2013); https://doi.org/10.1016/j.nanoen.2013.04.002
107. I.Venditti. *Materials*, **10** (2), 97 (2017); https://doi.org/10.3390/ma10020097
108. M.De, P.S.Ghosh, V.M.Rotello. *Adv. Mater*., **20** (22), 4225 (2008); https://doi.org/10.1002/adma.200703183
109. L.Bai, X.Wang, S.Tang, Y.Kang, J.Wang, Y.Yu, Z.-K.Zhou, C.Ma, X.Zhang, J.Jiang, P.K.Chu, X.-F.Yu. *Adv. Mater*., **30** (40), 1803641 (2018); https://doi.org/10.1002/adma.201803641
110. M.Caporali, M.Serrano-Ruiz, F.Telesio, S.Heun, G.Nicotra, C.Spinella, M.Peruzzini. *Chem. Commun*., **53** (79), 10946 (2017); https://doi.org/10.1039/c7cc05906j
111. M.Caporali, M.Serrano-Ruiz, F.Telesio, S.Heun, A.Verdini, A.Cossaro, M.Dalmiglio, A.Goldoni, M.Peruzzini. *Nanotechnology*, **31** (27), 275708 (2020); https://doi.org/10.1088/1361-6528/ab851e
112. Y.Li, W.Pei, J.He, K.Liu, W.Qi, X.Gao, S.Zhou, H.Xie, K.Yin, Y.Gao, J.He, J.Zhao, J.Hu, T.-S.Chan, Z.Li, G.Zhang, M.Liu. *ACS Catal*., **9** (12), 10870 (2019); https://doi.org/10.1021/acscatal.9b03506
113. Y.Peng, B.Lu, N.Wang, J.E.Lu, C.Li, Y.Ping, S.Chen. *ACS Appl. Mater. Interfaces*, **11** (27), 24707 (2019); https://doi.org/10.1021/acsami.9b05471
114. F.Shi, Z.Geng, K.Huang, Q.Liang, Y.Zhang, Y.Sun, J.Cao, S.Feng. *Adv. Sci*., **5** (8), 1800575 (2018); https://doi.org/10.1002/advs.201800575
115. M.Vanni, M.Serrano-Ruiz, F.Telesio, S.Heun, M.Banchelli, P.Matteini, A.M.Mio, G.Nicotra, C.Spinella, S.Caporali, A.Giaccherini, F.D'Acapito, M.Caporali, M.Peruzzini. *Chem. Mater*., **31** (14), 5075 (2019); https://doi.org/10.1021/acs.chemmater.9b00851
116. X.Wang, L.Bai, J.Lu, X.Zhang, D.Liu, H.Yang, J.Wang, P.K.Chu, S.Ramakrishna, X.-F.Yu. *Angew. Chem., Int. Ed.*, **58** (52), 19060 (2019); https://doi.org/10.1002/anie.201911696
117. Z.He, R.Liu, C.Xu, Y.Lai, W.Shan, J.Liu. *Appl. Catal. B*, **285**, 119775 (2021); https://doi.org/10.1016/j.apcatb.2020.119775
118. M.Valt, M.Caporali, B.Fabbri, A.Gaiardo, S.Krik, E.Iacob, L.Vanzetti, C.Malagù, M.Banchelli, C.D'Andrea, M.Serrano-Ruiz, M.Vanni, M.Peruzzini, V.Guidi. *ACS Appl. Mater. Interfaces*, **13** (37), 44711 (2021); https://doi.org/10.1021/acsami.1c10763

119. H.Qiao, H.Liu, Z.Huang, Q.Ma, S.Luo, J.Li, Y.Liu, J.Zhong, X.Qi. *Adv. Energy Mater*., **10** (44), 2002424 (2020); https://doi.org/10.1002/aenm.202002424
120. J.Hu, Z.Guo, P.E.McWilliams, J.E.Darges, D.L.Druffel, A.M.Moran, S.C.Warren. *Nano Lett*., **16** (1), 74 (2016); https://doi.org/10.1021/acs.nanolett.5b02895
121. Y.Xue, S.Min, F.Wang. *Int. J. Hydrogen Energy*, **44** (39), 21873 (2019); https://doi.org/10.1016/j.ijhydene.2019.06.087
122. G.Tang, F.Su, X.Xu, P.K.Chu. *Chem. Eng. J*., **392**, 123631 (2020); https://doi.org/10.1016/j.cej.2019.123631
123. X.Wang, B.Zhou, Y.Zhang, L.Liu, J.Song, R.Hu, J.Qu. *J. Alloys Compd*., **769**, 316 (2018); https://doi.org/10.1016/j.jallcom.2018.08.008
124. Q.Wu, M.Liang, S.Zhang, X.Liu, F.Wang. *Nanoscale*, **10** (22), 10428 (2018); https://doi.org/10.1039/c8nr01715h
125. M.Veselý, P.Marvan, J.Trejbal, V.Mazánek, J.Luxa, J.Šturala, Z.Sofer. *ACS Appl. Mater. Interfaces*, **12** (20), 22702 (2020); https://doi.org/10.1021/acsami.9b20618
126. M.Batmunkh, A.Shrestha, M.Bat-Erdene, J.Nine, C.J.Shearer, C.T.Gibson, A.D.Slattery, S.A.Tawfik, M.J.Ford, S.Dai, S.Qiao, J.G.Shapter. *Angew. Chem., Int. Ed*., **57** (10), 2644 (2018); https://doi.org/10.1002/anie.201712280
127. S.Moschetto, A.Ienco, G.Manca, M.Serrano-Ruiz, M.Peruzzini, A.Mezzi, M.Brucale, M.Bolognesi, S.Toffanin. *Dalton Trans*., **50** (33), 11610 (2021); https://doi.org/10.1039/d1dt02123k
128. R.Gao, X.Wang, X.Zhang, S.Zhang, X.Li, X.F.Yu, L.Bai. *Sep. Purif. Technol*., **316**, 123771 (2023); https://doi.org/10.1016/j.seppur.2023.123771
129. I.Pastorizo-Santos, L.M.Liz-Marzán. *Adv. Funct. Mater*., **19** (5), 679 (2009); https://doi.org/10.1002/adfm.200801566
130. Z.Zhang, X.Chen, X.Zhang, C.Shi. *Solid State Commun*., **139** (8), 403 (2006); https://doi.org/10.1016/j.ssc.2006.06.040
131. W.Yang, Y.Huang, J.Fan, Y.Yu, C.Yang, H.Li. *Nanoscale*, **8** (9), 4898 (2016); https://doi.org/10.1039/c6nr00208k
132. W.Li, W.Fu, S.Bai, H.Huang, X.He, W.Ma, H.Zhang, Y.Wang. *Electrochim. Acta*, **446**, 142082 (2023); https://doi.org/10.1016/j.electacta.2023.142082
133. Z.-Z.Luo, Y.Zhang, C.Zhang, H.T.Tan, Z.Li, A.Abutaha, X.-L.Wu, Q.Xiong, K.A.Khor, K.Hippalgaonkar, J.Xu, H.H.Hng, Q.Yan. *Adv. Energy Mater*., **7** (2), 1601285 (2017); https://doi.org/10.1002/aenm.201601285
134. Y.Lin, Y.Pan, J.Zhang. *Int. J. Hydrogen Energy*, **42** (12), 7951 (2017); https://doi.org/10.1016/j.ijhydene.2016.12.030
135. Q.Liang, F.Shi, X.Xiao, X.Wu, K.Huang, S.Feng. *ChemCatChem*, **10** (10), 2179 (2018); https://doi.org/10.1002/cctc.201701907
136. J.Wang, D.Liu, H.Huang, N.Yang, B.Yu, M.Wen, X.Wang, P.K.Chu, X.-F.Yu. *Angew. Chem., Int. Ed*., **57** (10), 2600 (2018); https://doi.org/10.1002/anie.201710859
137. Y.-J.Yuan, Z.-K.Shen, S.Song, J.Guan, L.Bao, L.Pei, Y.Su, S.Wu, W.Bai, Z.-T.Yu, Z.Ji, Z.Zou. *ACS Catal*., **9** (9), 7801 (2019); https://doi.org/10.1021/acscatal.9b02274
138. S.Yang, G.Chen, A.G.Ricciardulli, P.Zhang, Z.Zhang, H.Shi, J.Ma, J.Zhang, P.W.M.Blom, X.Feng. *Angew. Chem., Int. Ed*., **59** (1), 465 (2020); https://doi.org/10.1002/anie.201911428
139. H.Xiao, X.Du, M.Zhao, Y.Li, T.Hu, H.Wu, J.Jia, N.Yang. *Nanoscale*, **13** (15), 7381 (2021); https://doi.org/10.1039/d1nr00062d
140. D.Jia, Y.Zhang, Y.Xie, X.Zhang, H.Pan, Z.Chen. *Sens. Actuators, B: Chem*., **377**, 133095 (2023); https://doi.org/10.1016/J.SNB.2022.133095
141. Aid.M.Kuchkaev, A.V.Zhurenok, Air.M.Kuchkaev, A.V.Sukhov, V.S.Kashansky, M.M.Nikitin, K.A.Litvintseva, S.V.Cherepanova, E.Yu.Gerasimov, E.A.Kozlova, O.G.Sinyashin, D.G.Yakhvarov. *Kinet. Catal*., **65** (5), 579 (2024); https://doi.org/10.1134/S0023158424601979
142. E.Kovalska, J.Luxa, M.Melle-Franco, B.Wu, I.Marek, P.K.Roy, P.Marvan, Z.Sofer. *ACS Appl. Mater. Interfaces*, **12** (45), 50516 (2020); https://doi.org/10.1021/acsami.0c15525
143. L.Xiao, Q.Zheng, S.Luo, Y.Ying, R.Zhou, S.Zhou, X.Li, X.Ye, Z.Yu, Q.Xu, H.Liao, J.Xu. *Sci. Adv*., **10** (25), eadn2707 (2024); https://doi.org/10.1126/sciadv.adn2707
144. M.Zhao, R.Zhang, Z.Fu, H.Xiao, M.Bai, L.Zhang, J.Zhang, J.Jia, N.Yang. *Int. J. Hydrogen Energy*, **53**, 263 (2024); https://doi.org/10.1016/j.ijhydene.2023.12.084
145. B.Ni, X.Wang. *Adv. Sci*., **2** (7), 1500085 (2015); https://doi.org/10.1002/advs.201500085
146. M.A.Mahmoud, R.Narayanan, M.A.El-Sayed. *Acc. Chem. Res*., **46** (8), 1795 (2013); https://doi.org/10.1021/ar3002359
147. R.Narayanan, M.A.El-Sayed. *Nano Lett*., **4** (7), 1343 (2004); https://doi.org/10.1021/nl0495256
148. Q.S.Chen, F.J.Vidal-Iglesias, J.Solla-Gullón, S.G.Sun, J.M.Feliu. *Chem. Sci*., **3** (1), 136 (2011); https://doi.org/10.1039/C1SC00503K
149. Q.Zhang, J.Guan. *Adv. Funct. Mater*., **30** (31), 2000768; https://doi.org/10.1002/adfm.202000768
150. N.Cheng, L.Zhang, K.Doyle-Davis, X.Sun. *Electrochem. Energy Rev*., **2** (4), 539 (2019); https://doi.org/10.1007/s41918-019-00050-6
151. X.F.Yang, A.Wang, B.Qiao, J.Li, J.Liu, T.Zhang. *Acc. Chem. Res*., **46** (8), 1740 (2013); https://doi.org/10.1021/ar300361m
152. K.Miao, J.Qin, S.Lai, M.Luo, A.Kuchkaev, D.Yakhvarov, X.Kang. *Adv. Funct. Mater*., **35** (14), 2419989 (2025); https://doi.org/10.1002/adfm.202419989
153. J.Ma, L.Huang, K.Chen, J.Wang, X.Kang, X.Cao. *J. Colloid Interface Sci*., **652**, 1734 (2023); https://doi.org/10.1016/j.jcis.2023.08.202
154. K.Miao, J.Qin, J.Yang, X.Kang. *Adv. Funct. Mater*., **34** (33), 2316824 (2024); https://doi.org/10.1002/adfm.202316824
155. K.Miao, J.Wen, M.Luo, D.Xiang, Y.Jiang, D.Duan, Z.Jiang, W.Sun, B.Mei, Y.Xiong, X.Kang. *Nano Lett*., **24** (41), 12849 (2024); https://doi.org/10.1021/acs.nanolett.4c03182
156. G.Yang, D.Ma, L.Zhang, Y.Zhang, X.Tang, C.Li, C.Cui, X.Tong, Y.Xie, Y.Luo, L.Zhou. *Surf. Interfaces*, **70**, 106825 (2025); https://doi.org/10.1016/j.surfin.2025.106825
157. W.Zhong, J.Yue, R.Zhang, H.Huang, H.Huang, Z.Shen, L.Jiang, M.Xu, Q.Xia, Y.Cao. *Inorg. Chem*., **63** (2), 1035 (2024); https://doi.org/10.1021/acs.inorgchem.3c03320
158. X.Y.Li, M.Duan, P.Ou. *Nano Res*., **17** (4), 2360 (2024); https://doi.org/10.1007/s12274-023-6068-1
159. P.Vishnoi, U.Gupta, R.Pandey, C.N.R.Rao. *J. Mater. Chem. A*, **7** (12), 6631 (2019); https://doi.org/10.1039/c8ta08497a
160. D.Tofan, Y.Sakazaki, K.L.W.Mitra, R.Peng, S.Lee, M.Li, A.Velian. *Angew. Chem., Int. Ed*., **60** (15), 8329 (2021); https://doi.org/10.1002/anie.202100308
161. A.Ienco, G.Manca, M.Peruzzini, C.Mealli. *Dalton Trans*., **47** (48), 17243 (2018); https://doi.org/10.1039/C8DT03628D
162. Y.Zhao, H.Wang, H.Huang, Q.Xiao, Y.Xu, Z.Guo, H.Xie, J.Shao, Z.Sun, W.Han, X.-F.Yu, P.Li, P.K.Chu. *Angew. Chem., Int. Ed*., **55** (16), 5003 (2016); https://doi.org/10.1002/anie.201512038
163. Z.Qu, K.Wu, W.Meng, B.Nan, Z.Hu, C.-a.Xu, Z.Tan, Q.Zhang, H.Meng, J.Shi. *Chem. Eng. J*., **397**, 125416 (2020); https://doi.org/10.1016/j.cej.2020.125416
164. L.Wu, J.Wang, J.Lu, D.Liu, N.Yang, H.Huang, P.K.Chu, X.F.Yu. *Small*, **14** (29), 1801405 (2018); https://doi.org/10.1002/smll.201801405
165. K.L.W.Mitra, M.Riehs, A.Draguicevic, W.A.Swann, C.W.Li, A.Velian. *Angew. Chem., Int. Ed*., **62** (49), e202311575 (2023); https://doi.org/10.1002/anie.202311575
166. M.Vanni, M.Bellini, S.Borsacchi, L.Calucci, M.Caporali, S.Caporali, F.d'Acapito, M.Geppi, A.Giaccherini, A.Ienco, G.Manca, A.M.Mio, G.Nicotra, W.Oberhauser, M.Serrano-Ruiz, M.Banchelli, F.Vizza, M.Peruzzini. *J. Am. Chem. Soc*., **143** (27), 10088 (2021); https://doi.org/10.1021/jacs.1c01754
167. C.Chen, W.Ou, K.-M.Yam, S.Xi, X.Zhao, S.Chen, J.Li, P.Lyu, L.Ma, Y.Du, W.Yu, H.Fang, C.Yao, X.Hai, H.Xu, M.J.Koh, S.J.Pennycook, J.Lu, M.Lin, C.Su, C.Zhang, J.Lu. *Adv. Mater*.,

33 (35), 2008471 (2021); https://doi.org/10.1002/adma.202008471
168. X.Ren, L.Shi, Y.Li, S.Song, Q.Wang, S.Luo, L.Ren, H.Zhang, Y.Izumi, X.Peng, D.Philo, F.Ichihara, J.Ye. *ChemCatChem*., **12** (15), 3870 (2020); https://doi.org/10.1002/cctc.202000546
169. D.Liu, J.Wang, J.Lu, C.Ma, H.Huang, Z.Wang, L.Wu, Q.Liu, S.Jin, P.K.Chu, X.-F.Yu. *Small Methods*, **3** (7), 1900083 (2019); https://doi.org/10.1002/smtd.201900083
170. W.Zhai, Y.Chen, Y.Liu, T.Sakthivel, Y.Ma, S.Guo, Y.Qu, Z.Dai. *Adv. Funct. Mater*., **33** (25), 2301565 (2023); https://doi.org/10.1002/adfm.202301565
171. Z.K.Shen, Y.J.Yuan, L.Pei, Z.T.Yu, Z.Zou. *Chem. Eng. J*., **386**, 123997 (2020); https://doi.org/10.1016/j.cej.2019.123997
172. N.T.Suen, S.F.Hung, Q.Quan, N.Zhang, Y.J.Xu, H.M.Chen. *Chem. Soc. Rev*., **46** (2), 337 (2017); https://doi.org/10.1039/c6cs00328a
173. X.Chen, S.Shen, L.Guo, S.S.Mao. *Chem Rev*., **110** (11), 6503 (2010); https://doi.org/10.1021/cr1001645
174. S.E.Hosseini, M.A.Wahid. *Int. J. Energy Res*., **44** (6), 4110 (2020); https://doi.org/10.1002/er.4930
175. J.Zhu, L.Hu, P.Zhao, L.Y.S.Lee, K.Y.Wong. *Chem. Rev*., **120** (2), 851 (2019); https://doi.org/10.1021/acs.chemrev.9b00248
176. J.O.Abe, A.P.I.Popoola, E.Ajenifuja, O.M.Popoola. *Int. J. Hydrogen Energy*, **44** (29), 15072 (2019); https://doi.org/10.1016/j.ijhydene.2019.04.068
177. B.Sa, Y.L.Li, J.Qi, R.Ahuja, Z.Sun. *J. Phys. Chem. C*, **118** (46), 26560 (2014); https://doi.org/10.1021/jp508618t
178. Y.Gan, X.X.Xue, X.X.Jiang, Z.Xu, K.Chen, J.F.Yu, Y.Feng. *J. Phys. Condens. Matter*, **32** (2), 025202 (2020); https://doi.org/10.1088/1361-648X/ab482b
179. Q.Zhang, S.Huang, J.Deng, D.T.Gangadharan, F.Yang, Z.Xu, G.Giorgi, M.Palummo, M.Chaker, D.Ma. *Adv. Funct. Mater*., **29** (28), 1902486 (2019); https://doi.org/10.1002/adfm.201902486
180. P.Vishnoi, K.Pramoda, U.Gupta, M.Chhetri, R.G.Balakrishna, C.N.R.Rao. *ACS Appl. Mater. Interfaces*, **11** (31), 27780 (2019); https://doi.org/10.1021/acsami.9b06910
181. M.Zhu, Z.Sun, M.Fujitsuka, T.Majima. *Angew. Chem., Int. Ed*., **57** (8), 2160 (2018); https://doi.org/10.1002/anie.201711357
182. M.Zhu, S.Kim, L.Mao, M.Fujitsuka, J.Zhang, X.Wang, T.Majima. *J. Am. Chem. Soc*., **139** (37), 13234 (2017); https://doi.org/10.1021/jacs.7b08416
183. G.Provinciali, J.Filippi, A.Lavacchi, S.Caporali, M.Banchelli, M.Serrano-Ruiz, M.Peruzzini, M.Caporali. *ChemCatChem*., **15** (18), e202300647 (2023); https://doi.org/10.1002/cctc.202300647
184. X.X.Xue, S.Shen, X.Jiang, P.Sengdala, K.Chen, Y.Feng. *J. Phys. Chem. Lett*., **10** (12), 3440 (2019); https://doi.org/10.1021/acs.jpclett.9b00891
185. T.Wu, S.Zhang, K.Bu, W.Zhao, Q.Bi, T.Lin, J.Huang, Y.Li, F.Huang. *J. Mater. Chem. A*, **7** (38), 22063 (2019); https://doi.org/10.1039/c9ta07962a
186. T.Liang, S.Lenus, Y.Liu, Y.Chen, T.Sakthivel, F.Chen, F.Ma, Z.Dai. *Energy Environ. Mater*., **6** (2), e12332 (2023); https://doi.org/10.1002/eem2.12332
187. L.Zhang, Z.J.Zhao, J.Gong. *Angew. Chem., Int. Ed*., **56** (38), 11326 (2017); https://doi.org/10.1002/anie.201612214
188. S.Fang, M.Rahaman, J.Bharti, E.Reisner, M.Robert, G.A.Ozin, Y.H.Hu. *Nat. Rev. Methods Primers*, **3** (1), 61 (2023); https://doi.org/10.1038/s43586-023-00243-w
189. J.Liu, C.Guo, A.Vasileff, S.Qiao. *Small Methods*, **1** (1–2), 1600006 (2017); https://doi.org/10.1002/smtd.201600006
190. Z.Sun, N.Talreja, H.Tao, J.Texter, M.Muhler, J.Strunk, J.Chen. *Angew. Chem., Int. Ed*., **57** (26), 7610 (2018); https://doi.org/10.1002/anie.201710509
191. X.Zhu, S.Huang, Q.Yu, Y.She, J.Yang, G.Zhou, Q.Li, X.She, J.Deng, H.Li, H.Xu. *Appl. Catal. B*, **269**, 118760 (2020); https://doi.org/10.1016/j.apcatb.2020.118760
192. G.Zhou, J.Yang, X.Zhu, Q.Li, Q.Yu, W.El-alami, C.Wang, Y.She, J.Qian, HXu, H.Li. *J. Energy Chem*., **49**, 89 (2020); https://doi.org/10.1016/j.jechem.2020.01.020
193. X.Wang, J.He, J.Li, G.Lu, F.Dong, T.Majima, M.Zhu. *Appl. Catal. B*, **277**, 119230 (2020); https://doi.org/10.1016/j.apcatb.2020.119230
194. W.Gao, X.Bai, Y.Gao, J.Liu, H.He, Y.Yang, Q.Han, X.Wang, X.Wu, J.Wang, F.Fan, Y.Zhou, C.Li, Z.Zou. *Chem. Commun*., **56** (56), 7777 (2020); https://doi.org/10.1039/d0cc00805b
195. M.He, Z.Tian, H.Lin, G.Wang. *Small*, **20** (44), 2404162 (2024); https://doi.org/10.1002/smll.202404162
196. X.Zhu, G.Zhou, J.Yi, P.Ding, J.Yang, K.Zhong, Y.Song, Y.Hua, X.Zhu, J.Yuan, Y.She, H.Li, H.Xu. *ACS Appl. Mater. Interfaces*, **13** (33), 39523 (2021); https://doi.org/10.1021/acsami.1c12692
197. Y.Xu, W.Zhang, G.Zhou, M.Jin, X.Li. *J. Colloid Interface Sci*., **616**, 641 (2022); https://doi.org/10.1016/J.JCIS.2022.01.185
198. J.Hu, T.Yang, X.Yang, J.Qu, Y.Cai, C.M.Li. *Small*, **18** (7), 2105376 (2022); https://doi.org/10.1002/smll.202105376
199. J.Huang, X.Guo, J.Yang, L.Wang. *J. CO_2 Utilization*, **38**, 32 (2020); https://doi.org/10.1016/j.jcou.2020.01.008
200. G.Zhang, Y.Li, C.He, X.Ren, P.Zhang, H.Mi. *Adv. Energy Mater*., **11** (11), 2003294 (2021); https://doi.org/10.1002/aenm.202003294
201. X.Guo, H.Du, F.Qu, J.Li. *J. Mater. Chem. A*, **7** (8), 3531 (2019); https://doi.org/10.1039/c8ta11201k
202. L.Zhang, L.X.Ding, G.F.Chen, X.Yang, H.Wang. *Angew. Chem., Int. Ed*., **58** (9), 2612 (2019); https://doi.org/10.1002/anie.201813174
203. S.Bian, M.Wen, J.Wang, N.Yang, P.K.Chu, X.F.Yu. *J. Phys. Chem. Lett*., **11** (3), 1052 (2020); https://doi.org/10.1021/acs.jpclett.9b03507
204. D.Liu, J.Wang, S.Bian, Q.Liu, Y.Gao, X.Wang, P.K.Chu, X.F.Yu. *Adv. Funct. Mater*., **30** (24), 2002731 (2020); https://doi.org/10.1002/adfm.202002731
205. Z.K.Shen, Y.J.Yuan, P.Wang, W.Bai, L.Pei, S.Wu, Z.T.Yu, Z.Zou. *ACS Appl. Mater. Interfaces*, **12** (15), 17343 (2020); https://doi.org/10.1021/acsami.9b21167
206. Y.T.Liu, D.Li, J.Yu, B.Ding. *Angew. Chem., Int. Ed*., **131** (46), 16591 (2019); https://doi.org/10.1002/anie.201908415
207. C.Wang, J.Gao, J.G.Zhao, D.J.Yan, X.D.Zhu. *Small*, **16** (18), 1907091 (2020); https://doi.org/10.1002/smll.201907091
208. P.Qiu, C.Xu, N.Zhou, H.Chen, F.Jiang. *Appl. Catal. B: Environ*., **221**, 27 (2018); https://doi.org/10.1016/j.apcatb.2017.09.010
209. J.Lai, H.Liu, L.X.Ding, J.Wang, G.F.Chen, H.Wang. *Adv. Energy Mater*., **14** (28), 2303963 (2024); https://doi.org/10.1002/aenm.202303963
210. H.Liu, G.Hai, L.X.Ding, H.Wang. *Angew. Chem., Int. Ed*., **62** (19), e202302124 (2023); https://doi.org/10.1002/anie.202302124
211. P.Ou, X.Zhou, F.Meng, C.Chen, Y.Chen, J.Song. *Nanoscale*, **11** (28), 13600 (2019); https://doi.org/10.1039/c9nr02586c
212. G.Xu, H.Li, A.S.R.Bati, M.Bat-Erdene, J.Nine, D.Losic, Y.Chen, J.G.Shapter, M.Batmunkh, T.Ma. *J. Mater. Chem. A*, **8** (31), 15875 (2020); https://doi.org/10.1039/d0ta03237a
213. S.Bian, Q.Liu, X.Zhang, C.Ma, Y.Zhang, Z.Cheng, Y.Kang, W.Lu, P.K.Chu, X.-F.Yu, J.Wang. *Small*, **18** (39), 2203284 (2022); https://doi.org/10.1002/smll.202203284
214. H.Liu, K.Hu, D.Yan, R.Chen, Y.Zou, H.Liu, S.Wang. *Adv. Mater*., **30** (32), 1800295 (2018); https://doi.org/10.1002/adma.201800295